Non-steady-state Stomatal Conductance Modeling and Its Implications: From Leaf to Ecosystem

Ke Liu[1], Yujie Wang[1], Troy Magney[2], and Christian Frankenberg[1,3]

[1]Division of Geological and Planetary Sciences, California Institute of Technology, Pasadena, California 91125, USA
[2]Department of Plant Sciences, University of California, Davis, CA 95616, USA
[3]Jet Propulsion Laboratory, California Institute of Technology, Pasadena, California 91109, USA

Correspondence: Ke Liu (klliu@caltech.edu) and Christian Frankenberg (cfranken@caltech.edu)

Abstract. Accurate and efficient modeling of stomatal conductance (g_s) has been a key challenge in vegetation models across scales. Current practice of most land surface models (LSMs) assumes steady-state g_s and predicts stomatal responses to environmental cues as immediate jumps between stationary regimes. However, the response of stomata can be orders of magnitude slower than that of photosynthesis, and often cannot reach a steady state before the next model time-step, even on half-hourly time scales. Here, we implemented a simple dynamic g_s model in the vegetation module of an LSM developed within the Climate Modeling Alliance, and investigated the potential biases caused by the steady state assumption from leaf to canopy scales. In comparison with steady-state models, the dynamic model better predicted the coupled temporal response of photosynthesis and stomatal conductance to changes in light intensity using leaf measurements. In ecosystem flux simulations, while the impact of g_s hysteresis response may not be substantial in terms of monthly integrated fluxes, our results highlight the importance of considering this effect when quantifying fluxes in the mornings and evenings, and interpreting diurnal hysteresis patterns observed in ecosystem fluxes. Simulations also indicate that the biases in the integrated fluxes are more significant when stomata exhibit different speeds for opening and closure. Furthermore, prognostic modeling can bypass the A-C_i iterations required for steady-state simulations and can be robustly run with comparable computational costs. Overall, our study demonstrates the implications of dynamic g_s modeling in improving the accuracy and efficiency of LSMs, and for advancing our understanding of plant-environment interactions.

1 Introduction

Modeling stomatal conductance (g_s), the opening and closure of tiny pores on leaves, is one of the key elements and challenges in land surface models (LSMs). Stomata regulate the gas exchange rates of plants, allowing the uptake of CO_2 for photosynthetic assimilation while constraining water loss through transpiration (Berry et al., 2010; Damour et al., 2010). The behavior of stomata, especially their responses to environmental variations, plays a significant role in determining the fluxes of carbon, water, and energy between vegetated surfaces and the atmosphere (Berry et al., 2010; Buckley, 2017). Therefore, accurate and efficient modeling of g_s is important for understanding the current Earth system and projecting future changes.

Stomatal conductance has been traditionally predicted with empirical models, relating g_s to photosynthesis rate and environmental cues with estimated parameters from statistical regressions (Ball et al., 1987; Leuning, 1990, 1995; Medlyn et al., 2011;

25 Damour et al., 2010). Efforts have also been made to constrain stomatal behavior from the principle of optimizing the trade-offs between carbon gain with the related penalty of stomatal opening (Wolf et al., 2016; Venturas et al., 2018; Wang et al., 2020). Additional understanding of stomatal response includes plant hydraulic models that consider the transport of water from soil through plants into the atmosphere (soil-plant-atmosphere continuum, SPAC) (Sperry et al., 1998, 2002; Bonan et al., 2014). However, most existing stomatal models, especially those currently used to scale from leaf to canopy level and implemented

30 in LSMs, assume steady states (Vialet-Chabrand et al., 2017). They predict the opening and closure of stomata in stationary regimes, modeling stomatal response to environmental variations as immediate jumps between states (Vialet-Chabrand et al., 2013).

While steady-state models assume that stomatal conductance changes instantaneously with the environment, the temporal response of stomata in reality can often be an order of magnitude slower than the biochemical response of photosynthesis (Pearcy

35 and Seemann, 1990; Vialet-Chabrand et al., 2013). Plants can experience frequent environmental changes on a timescale of seconds, such as light fluctuations due to cloud cover and canopy shading. Meanwhile, stomatal response times vary from minutes to more than an hour. Thus, a steady state is often not reached when environmental conditions change faster than stomata can respond to (Lawson and Blatt, 2014; Vialet-Chabrand et al., 2017). This slower response of g_s could further impose regulations on assimilation rate via its effects on intercellular CO_2 concentration (C_i), notably under rapidly-changing incident radiation

40 in natural environments (Kaiser and Kappen, 2000; Vialet-Chabrand et al., 2017). The mismatch and interaction of photosynthesis and stomatal response could lead to temporal variations in water use efficiency (WUE) as well (Lawson et al., 2011; Venturas et al., 2018). These can all lead to biases and it is important to consider non-steady-state temporal responses of g_s for more accurate predictions of ecosystem fluxes. Additionally, the inclusion of this factor may also contribute to the hysteresis of plant responses and ecosystem fluxes observed in natural diurnal cycles (Vialet-Chabrand et al., 2013), e.g. evapotranspiration

45 (ET) rates tend to be higher in the afternoon under the same incoming radiation, while canopy conductance overall decreases. These patterns have often been attributed solely to the asymmetry of meteorological variables, especially in temperature and vapor pressure deficit (Zeppel et al., 2004; Bai et al., 2015; Gimenez et al., 2019; Oogathoo et al., 2020; Lin et al., 2019).

The current practice of employing g_s models that assume steady-states requires iterations to converge to stable solutions at each simulation step. At the leaf level, this typically involves two nested iteration loops, first to solve the coupled photosynthesis-

50 stomatal conductance ($A_n - g_s$) model for C_i, and then to solve the leaf energy budget for leaf temperature (Collatz et al., 1991; Bonan et al., 2018), as g_s affects latent heat flux through transpiration. This approach can potentially lead to numerical issues (Sun et al., 2012) and increased computational costs, particularly when upscaling with complex canopies, where angular distribution setups are necessary (Wang and Frankenberg, 2022). However, by utilizing prognostic updates of variables, a dynamic model could simplify simulation steps and improve computational efficiency, enabling runs at finer temporal resolutions.

55 Moreover, accurate parameter estimation with steady-state models (e.g. linear fitting for the slope g_1 in empirical models) necessitates measurements to be taken after reaching each equilibrium (Leuning, 1990; Miner et al., 2017). Depending on wide-ranging stomatal response speeds (McAusland et al., 2016), obtaining one accurate response curve could take several hours (Liozon et al., 2000; Duarte et al., 2016). Too short of a time step could result in overestimation, underestimation, or unstable results of parameter estimates with steady-state assumptions (Xu and Baldocchi, 2003), which may often be overlooked (Miner

et al., 2017). Alternatively, estimates can be approached with a prognostic model by fitting the entire response curve, where steady-state measurements are not fundamentally necessary.

Limitations of steady-state stomatal modeling have driven efforts to develop dynamic models, primarily at the leaf level (Damour et al., 2010; Vialet-Chabrand et al., 2017). Based on observed variations of g_s, analytical equations of sigmoidal or exponential response have been commonly used (Naumburg and Ellsworth, 2000; Noe and Giersch, 2004; Vialet-Chabrand et al., 2013; Vialet-Chabrand et al., 2017; Martins et al., 2016; McAusland et al., 2016); directly adding time-dependent terms into traditional steady-state models has also been proposed (Matthews et al., 2018). While these models have demonstrated effective performance in reproducing leaf-level responses to light intensity in controlled conditions, the impacts of including temporal stomatal dynamics on the simulations of larger-scale fluxes under coupled variations in the natural environment (e.g., transpiration in the coupled diurnal cycles of radiation, temperature, and vapor pressure deficit (VPD)) have not been investigated. This may be partly due to the parametrization and complexity of many models optimized for leaf-scale predictions (Kirschbaum et al., 1988; Vialet-Chabrand et al., 2016), which constrains the feasibility of scaling them to the canopy level in LSMs.

In this study, we aim to: 1) implement a simplified dynamic stomatal model in the CliMA-Land model, i.e., the land component of a new generation Earth system model within the Climate Modeling Alliance (CliMA); 2) test model performance on leaf-level measurements and demonstrate an alternative method of parameter estimation with the non-steady-state model in a Bayesian nonlinear inversion framework; 3) compare simulations of the dynamic model with traditional steady-state modeling, primarily focusing on the differences in predictions of canopy fluxes and responses to coupled environmental variations on different time scales.

2 Methods and Materials

2.1 Model framework

2.1.1 Dynamic stomatal modeling

The current steady-state modeling approach in LSMs requires convergence of nested iteration loops to solve leaf fluxes at each time step (Figure 1a) (Bonan et al., 2018). In this study, we proposed to replace the inner loop for steady solutions of the coupled photosynthesis-stomatal conductance ($A_n - g_s$) model with prognostic updates of g_{sw} at finer time steps (Figure 1b).

At each step, instead of assuming a initial C_i and iterating until convergence, our framework starts with an initial g_{sw} (e.g. for the first time step of a diurnal simulation from midnight, this can be set as the minimal conductance in dark). Then solves A_n and C_i with biochemical demand and diffusive supply of internal CO_2 (Figure 1). For instance, when applying the Farquhar photosynthesis model for C3 plants (Farquhar et al., 1980), with a given g_{sw}, the RubisCO limited rate (A_c) and light limited

rate A_j are calculated using:

$$A_c = V_{cmax} \cdot \frac{C_i - \Gamma^*}{C_i + K_m} = g_{lc} \cdot (C_a - C_i) + R_d, \tag{1}$$

$$A_j = J \cdot \frac{C_i - \Gamma^*}{4C_i + 8\Gamma^*} = g_{lc} \cdot (C_a - C_i) + R_d. \tag{2}$$

where the middle parts in Eq. 1 and Eq. 2 represent the biochemical demand, and the right part represents the diffusive supply limitation of photosynthesis. V_{cmax} is the maximum carboxylation rate, C_a is the ambient CO_2 concentration, R_d is the respiration rate, Γ^* is the CO_2 compensation point with the absence of respiration, J is the electron transport rate, K_m is the Michaelis-Menten's coefficient, g_{lc} is the leaf total conductance to CO_2, which can be calculated using: $g_{lc}^{-1} = g_{bc}^{-1} + 1.6 g_{sw}^{-1} + g_m^{-1}$, with g_{bc} the boundary conductance to CO_2 and g_m the mesophyll conductance. Note that computing A_c or A_j requires solving for C_i first. With a known g_{lc} from g_{sw} at each time-step, rearranging Eq. 1 and Eq. 2 allows for the analytical solution of C_i, A_c and A_j, respectively.

For prognostic updates of g_{sw}, we implemented a simplified dynamic model, adapted from previous studies on leaf-level prognostic modeling (Kirschbaum et al., 1988; Rayment et al., 2000; Noe and Giersch, 2004; Vialet-Chabrand et al., 2016):

$$\frac{\Delta g_t}{\Delta t} = \frac{(g_{ss} - g_t)}{\tau} \tag{3}$$

where Δt is the time step of the simulation, g_t represents the conductance at the current time step, g_{ss} is the target conductance calculated with steady-state models at the current conditions, and τ is the time constant, representing the time scale of stomatal responses. In this study, we used the Ball-Berry model (Ball et al., 1987) to compute the g_{ss} for leaf level simulations for simplicity and the Medlyn model (Medlyn et al., 2011) for the canopy scale simulations, as the vegetation trait dataset (De Kauwe et al., 2015) we employed for our study region is only available for the Medlyn parameters. We should note that the selection of the empirical stomatal model is of minor relevance to our primary findings, as our study focuses on the differences between steady-state and prognostic schemes only.

As indicated in the flow chart (Figure 1), our dynamic modeling avoids nested iterations for steady solutions while requires updates of variables at finer time steps (e.g. 5-10 min, compared to 30 or 60 min time steps of current LSMs) for the stability of simulations, which we tested and discussed in Section 2.3.2 and 3.3. The prognostic updates of leaf temperature can be implemented accordingly, but as it is not within the scope of this study, we prescribed the leaf temperature updates with measurements in our simulations.

2.1.2 Implementation in LSM

CliMA Land (https://github.com/CliMA/Land), a new generation LSM, is highly modularized and offers flexible model schemes (Wang et al., 2021, 2023), enabling easy implementation and assessment of the dynamic stomatal model across scales. To test the model performance and compare simulations with different stomatal modeling schemes, we implemented our non-steady-state framework in CliMA Land. More information on the CliMA Land configuration can be found in the supplementary material (Section S1.1) and Wang et al. (2021, 2023).
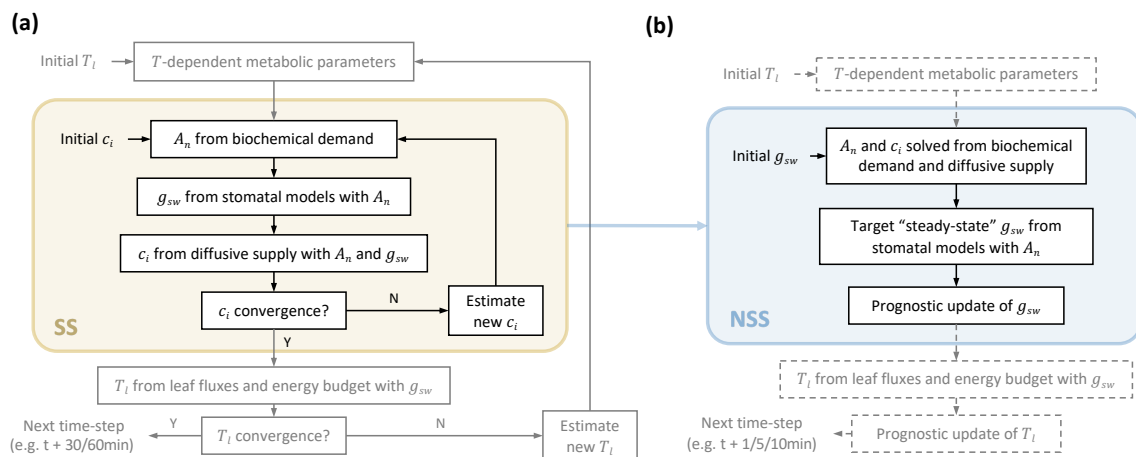
Figure 1. Comparison of leaf flux calculation flows in (a) steady-state (SS) and (b) non-steady-state (NSS) dynamic modeling. (a) illustrates the two nested loops at each time step in the current practice of steady-state framework, adapted from Bonan et al. (2018). The inner iteration in the light yellow box represents the flow of solving the coupled photosynthesis-stomatal conductance (A_n-g_s) model for C_i. The outer solves the leaf energy budget for leaf temperature (T_l). The focus of this study is to implement and compare a dynamic modeling framework to the A_n-g_s model, illustrated in light blue box in (b), where, instead of iterating for steady solutions, g_{sw} is updated prognostically at finer time steps, based on environmental conditions and a simplified dynamic model (Section 2.1.1). This NSS framework of modeling g_{sw} also allows prognostic updates of T_l. As its implementation is not within the scope of this study, related flows are shown in dashed parts.

2.2 Performance on leaf level measurements

2.2.1 Leaf gas exchange

To test our model and determine key parameters, we recorded light response curves of grape (*Vitis vinifera*) and walnut (*Juglans regia cv.*) leaves using a LI-6800 portable photosynthesis system (LI-COR, Inc., Lincoln, NE, USA). Saplings of *Vitis vinifera* and *Juglans regia cv.* were planted in 5-gallon pots with UC soil mix. 44.4 mL of Osmocote® Smart-Release® Plant Food Plus fertilizer were added to each pot. The plants were grown in a UC Davis lath house. The plants were watered to maintain around 75 percent of completely saturated soil by weight (details in Meeker et al. (2021)). The youngest, fully expanded, intact leaf was chosen and dark-adapted for 30 min. During the measurements, the photosynthetic photon flux density (PPFD) was sequentially increased following the gradient of 50, 100, 200, 400, 600, 900, 1200, 1500, 1800 μmol m^{-2} s^{-1}, with a time step of 30 min at each light level. The chamber air temperature was set at 25 °C; CO2 partial pressure was controlled at 400 ppm; the relative humidity in the chamber was maintained around 50%.

2.2.2 Parameter optimization

We applied a Bayesian nonlinear inversion framework (Rodgers, 2000; Dutta et al., 2019) to jointly fit the response curves of the net photosynthetic assimilation (A_n) and stomatal conductance (g_s) for each leaf with the non-steady-state model. The forward problem in this case can be represented as follows:

$$y = \mathcal{F}(X; b) + \epsilon; \tag{4}$$

where y represent the measurements, i.e. the light response curves of both A_n and g_s (see Section 2.2.1); $\mathcal{F}$ represents the forward model, CliMA-Land with the dynamic g_s model (see Section 2.1); X is the state vector of parameters to be retrieved, which in our case includes: the maximum carboxylation rate (V_{cmax}), the slope (g_1) and the minimum conductance (g_0) of the BB model, the mesophlly conductance (g_m) (Sun et al., 2014), and the time constant (τ). We also included a scaling factor for A_n, to account for variations in the respiration rate and the ratios between CO_2 and H_2O fluxes; b is the vector of other parameters that have influences the measurements, are known to some accuracy but not intended to be retrieved, e.g. the ratio between J_{max} (the maximum electron transport rate) and V_{cmax}, which is assumed to be 1.6 in this study but may vary across conditions (Medlyn et al., 2002); and ϵ is the error term.

The Levenberg–Marquardt (LM) iterations (Levenberg, 1944; Marquardt, 1963; Rodgers, 2000) were utilized to solve the nonlinear inversion problem and find the best estimate of key parameters:

$$x_{i+1} = x_i + \left((1+\gamma)S_a^{-1} + K_i^T S_\epsilon^{-1} K_i\right)^{-1} \left(K_i^T S_\epsilon^{-1} [y - F(X_i)] - S_a^{-1} [x_i - x_a]\right) \tag{5}$$

where x_a is the prior estimate of the state (in this study, V_{cmax}: 70 μmol m^{-2}s^{-1}, g_1: 9, g_0: 0.03 mol H_2O m^{-2} s^{-1}, g_m: 0.4 mol CO_2 m^{-2} s^{-1}, τ: 600 s, $scaling_A$: 1); S_a is the prior covariance matrix, assumed to be purely diagonal, with Gaussian uncertainties in the prior state (the assumed prior standard deviation of V_{cmax}: 30, g_1: 3, g_0: 0.005, g_m: 0.02, τ: 100, $scaling_A$, 0.01). K_i is the Jacobian matrix at the ith iteration. γ is adjusted at each step, ensuring that each update of the state vector moves towards minimizing the cost function. S_ϵ is the error covariance matrix; in our case, errors were assumed to be mainly from measurement uncertainties and calculated based on the standard deviation and mean of the ΔCO_2 and ΔH_2O in LI-6800 measurements.

2.2.3 Uncertainties in traditional parameter estimation

To illustrate the influence of time steps on parameter estimation in the traditional method, which assumes steady states, we used the NSS model to generate leaf response curves to the same PPFD sequence but with different time intervals. For example, in the 5-min time step simulation, light intensity input jumped every 5 minutes, and measurements were assumed to be taken right before the next jump, following the traditional method. We then employed these curves to calculate the estimated g_1 and g_0 values using the traditional linear fitting method for the Ball-Berry model. The potential biases were assessed by comparing fitted parameters with different applied time steps.

2.3 Comparison of models in diurnal cycles

To assess the potential bias of the current steady-state modeling in LSMs, we compared the predictions of surface fluxes from models with different assumptions under natural environmental variations. We evaluated and compared the simulation results on both the leaf and canopy flux scales.

2.3.1 Environmental drivers and plant traits

As the light intensity tends to be the most rapidly changing environmental condition that stomata response to, we employed high temporal resolution radiation measurements in the field as the incoming irradiance inputs and ran CliMA Land with both setups. Photosynthetically active radiation (PAR) in a crop field (42.481677°N, 93.523521°W) was recorded with a LI-190R quantum sensor (LI-COR, Inc., Lincoln, NE, USA) at 1 s temporal resolution during August 2017.

In addition to the fluctuations of total incoming photon density that the PAR sensor can provide, canopies in natural environments also experience variations in the fraction of direct and diffuse components in the total radiation. This variation affects the distribution of PAR received by individual leaves across different layers of the canopy structure (Durand et al., 2021). To account for this effect, we employed an empirical fitting with the hourly radiation data from ERA5 (Figure S2), to estimate the partitioning between the direct and diffuse radiation (Boland et al., 2001). The empirical relationship was then applied to high temporal resolution PAR measurements to obtain the direct and diffuse components in the recorded total radiation, which were used as inputs for simulations at the canopy scale.

Other meteorological variables (e.g. air temperature, dew-point temperature, volumetric soil water, wind speed etc.) were extracted from the ERA5 hourly reanalysis dataset (Hersbach et al., 2018) and input as environmental drivers for the simulations on the canopy scale. Linear interpolations were applied for runs at sub-hourly time steps. Key plant traits (e.g. V_{cmax}, g_1, leaf area index (LAI)) were extracted from several globally gridded datasets using GriddingMachine (Wang et al. 2022; Croft et al. 2020; Butler et al. 2017; Luo et al. 2021; De Kauwe et al. 2015; Yuan et al. 2011; He et al. 2012, ; also see Wang et al. (2023) for detailed information on global scale datasets used in CliMA-Land).

2.3.2 Model simulations

We ran the CliMA Land surface flux simulations with different stomatal modeling schemes to assess the effects of g_s temporal response on model predictions. In the SS runs, iterations were employed to converge to steady-state solutions at each time step. For NSS mode, previous studies have observed different time constants for stomatal opening (τ_{op}) and closure (τ_{cl}) in various species, as well as a positive correlation between τ_{op} and τ_{cl}, with of the τ_{op}/τ_{cl} ratio varying from around 1/3 to 3 (McAusland et al., 2016; Vico et al., 2011; Ozeki et al., 2022). Based on the average time constant retrieved from the leaf response curves in Section 2.2.1 and 2.2.2 as well as previous estimates on the time constant variations (Vialet-Chabrand et al., 2013; McAusland et al., 2016; Vialet-Chabrand et al., 2017; Vico et al., 2011; Ozeki et al., 2022), we tested several sets of τ_{op} and τ_{cl} varying from 300 s to 900 s, including (a) $\tau_{op} = \tau_{cl} = 900$ s, as the base comparison; (b) $\tau_{op} > \tau_{cl}$, with τ_{op}/τ_{cl} ratios varying from 1.2 to 3, e.g. $\tau_{op} = 900$ s, $\tau_{cl} = 300$ s; (c) $\tau_{cl} > \tau_{op}$, with τ_{cl}/τ_{op} ratios from 1.2 to 3, e.g. $\tau_{op} = 300$ s, $\tau_{cl} = 900$ s.

For the leaf-scale runs, we used the key parameters retrieved in previous sections and tested model predictions for an ideal clear-sky day. To investigate the differences in ecosystem fluxes, we ran and assessed the NSS and SS simulations using a time step of 1 minute, with the inputs of meteorological drivers and plant traits at the location of the PAR measurement for the month of August 2017. Meteorological variables are updated at each time step. In order to further evaluate the potential contribution of g_s hysteresis to the observed diurnal hysteresis of ecosystem fluxes, we compared the standard runs with the model predictions where environmental variables (e.g. temperature, VPD, soil water content (SWC), etc.) were held constant over the daytime (as the mean of daytime values in each day). This approach allowed us to isolate the effect of hysteresis in g_s response and assess its potential contribution to the observed diurnal hysteresis of canopy and ecosystem fluxes.

Furthermore, to test the stability of prognostic modeling and assess the computational cost, we compared NSS simulations using different time steps, as well as the SS simulation run at a time step of 30 min, which is commonly used in current LSMs. This enabled us to evaluate the sensitivity of NSS predictions to the time step used, as well as compare the computational cost for stable NSS runs and standard SS simulations. We resampled the environmental drivers from ERA5 and the PAR sensor to match the temporal resolution of the simulations, while maintaining constant average values for each diurnal cycle across simulations with different time steps.

3   Results

3.1   Model performance and parameter estimates on leaf measurements

With the parameters estimated from the LM inversion framework, the non-steady-state model well predicted the temporal responses of g_{sw} and A_n (Figure 2). The model was able to capture the gradual increases of g_{sw} and A_n after each step change in $APAR$, and the reproduced curves were close to the measurements, with all R^2 higher than 0.98. Fitted time constant τ showed a variation between the two example leaves (292 s and 2028 s for the *Vitis vinifera* leaf and the *Juglans regia cv.* leaf, respectively). The relative difference in the time constant matched with the variations of response speed observed in the measured response curves (Figure 2). Compared to the SS model, the dynamic model provided more accurate prediction to the temporal responses. The improvements in R^2 were more prominent in the predictions of the *Juglans regia cv.* leaf responses, which have a larger time constant, than in those of the *Vitis vinifera* leaf. Other parameters estimated for the *Vitis vinifera* leaf include V_{cmax}: 71 µmol m^{-2}s^{-1}, g_1: 11.3, g_0: 0.023 mol H$_2$O m^{-2} s^{-1}, g_m: 0.18 mol CO$_2$ m^{-2} s^{-1}, $scaling_A$: 1.1; for the *Juglans regia cv.* leaf, V_{cmax}: 152 µmol m^{-2}s^{-1}, g_1: 3.9, g_0: 0.052 mol H$_2$O m^{-2} s^{-1}, g_m: 0.34 mol CO$_2$ m^{-2} s^{-1}, $scaling_A$: 1.0.

The dynamic model was also able to better capture the temporal variations of internal CO$_2$ concentration (Figure 3). Particularly, the NSS model reproduced the undershooting of the intercellular CO$_2$ concentration (C_i) after each step change in light intensity, which resulted from the differences in the speed of g_s and A_n responses and their interactions. As shown in the measured time series (Figure 2), after each increase in the incident light, photosynthesis was able to respond almost instantaneously, leading to a rapid decrease in C_i, while stomata opened gradually, slowly bringing up C_i over time. This then led to a gradual rise of A_n after the initial rapid response, indicating the regulation of g_s on A_n through its impacts on the internal
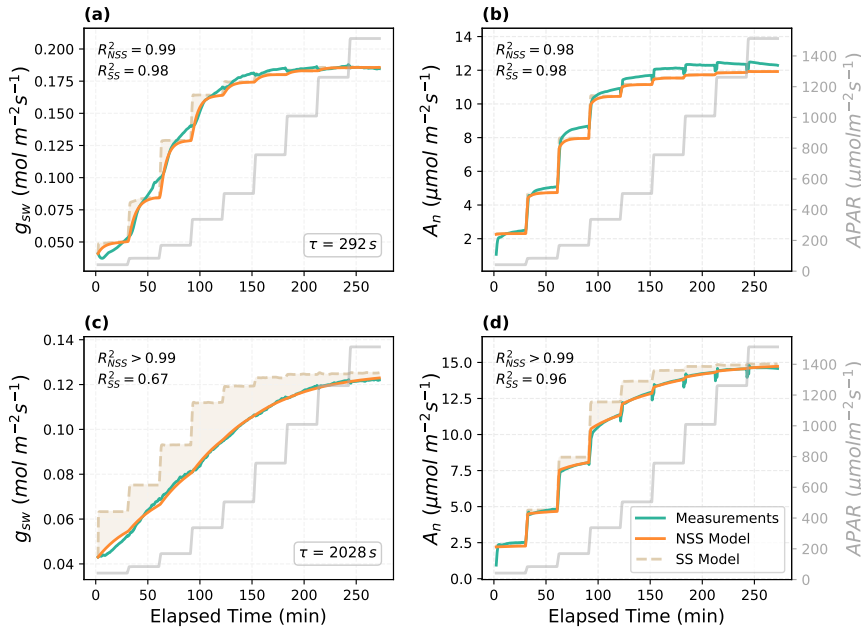
Figure 2. Modeled and measured temporal responses of the stomatal conductance (g_{sw}) and net photosynthesis rate (A_n) to the step changes in APAR for different leaves. The shaded area indicates the difference between the prediction of the steady-state (SS) model and the non-steady-state (NSS) dynamic model. (a-b) The temporal responses of the *Vitis vinifera* leaf, (c-d) the *Juglans regia cv.* leaf.

CO_2 supply. In the meantime, the increasing A_n further promoted the opening of stomata with a higher internal CO_2 demand, demonstrating their coupled responses to environmental variations.

With the dynamic model and optimized parameters that accurately reproduced the measured leaf responses, we investigated the influence of time steps used in light response curves (i.e. the length of intervals between step changes in light intensity) on parameter estimates obtained with traditional methods (Figure 4). The results showed that, particularly for the *Juglans regia cv.* leaf that has a long time constant over 2000 s, the values and relationship between the Ball-Berry index and g_{sw} varied significantly depending on the time step used, resulting in notable uncertainties in fitted g_1 and g_0 with too short of a interval to reach equilibrium. This also suggested that obtaining reliable estimates for this leaf using the traditional method could require more than an hour for stable readings at each step.

3.2 Model comparison in diurnal cycles

3.2.1 Leaf responses

To compare NSS and SS models over the course of a day, we evaluated the differences in their predictions of leaf responses to an ideal diurnal cycle of light with other environmental conditions (e.g. temperature, VPD, CO_2) held constant (Figure 5).
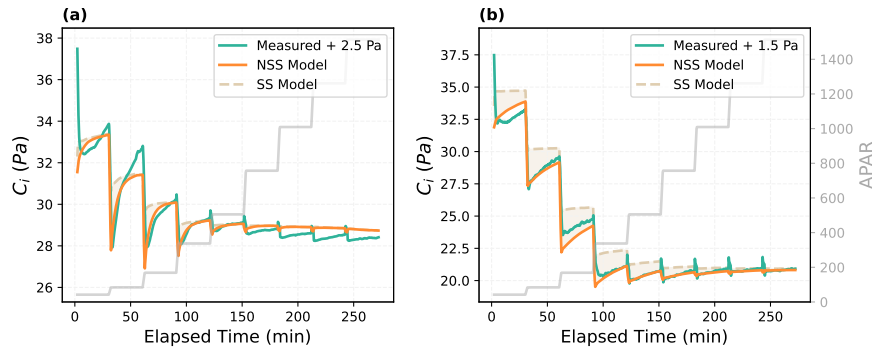
Figure 3. Modeled and measured temporal responses of intercelluar CO_2 concentration (C_i) for (a) the *Vitis vinifera* leaf and (b) the *Juglans regia cv.* leaf. As indicated in labels, measured curves were shifted to illustrate the comparison of modelled and measured response patterns, as the absolute values are not directly comparable due to different assumptions of LI-6800 and CliMA-Land in calculating the internal CO_2. The shaded area indicates the difference between the prediction of the steady-state (SS) model and the non-steady-state (NSS) dynamic model.
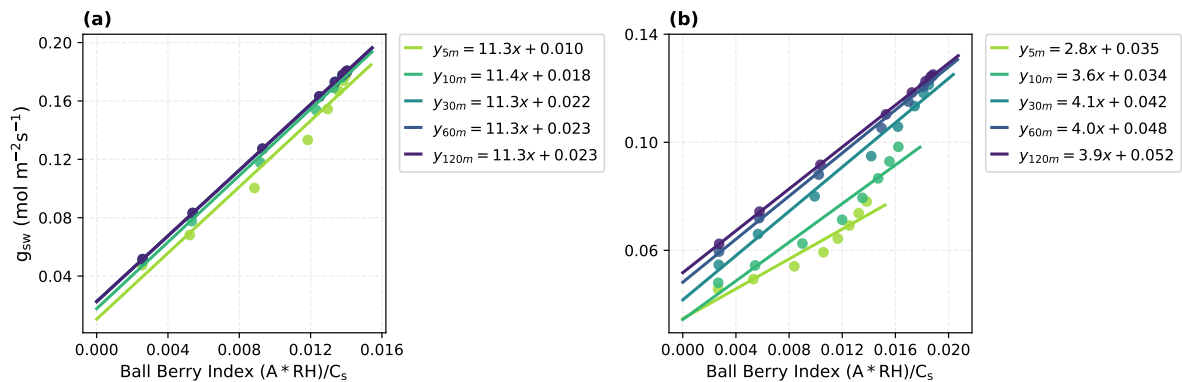
Figure 4. Parameter estimates for the Ball-Berry model with the traditional linear fitting method using model-reproduced response curves with different time steps (5 min, 10 min, 30 min, 60 min, 120 min). (a) fitting results for the *Vitis vinifera* leaf, (b) the *Juglans regia cv.* leaf. Corresponding Ball-Berry index and g_{sw} are plotted, along with the fitted lines and parameters (i.e. the Ball-Berry slope, g_1, and the intercept, namely, the minimum conductance, g_0).

Results showed that compared to NSS, the SS model predicted a higher A_n and g_s in the morning, as it assumed the stomata could respond immediately to an increase in light, whilst in the more realistic NSS simulation, the gradual opening of stomata limited the CO_2 supply for photosynthesis with a lower C_i. The opposite was true for the afternoon, but the overestimation of A_n and g_s in SS modeling in the morning was more significant than the underestimation in the afternoon, leading to slightly higher diurnally-integrated predictions than those of the NSS model. This was due to the fact that in the course of sunset,
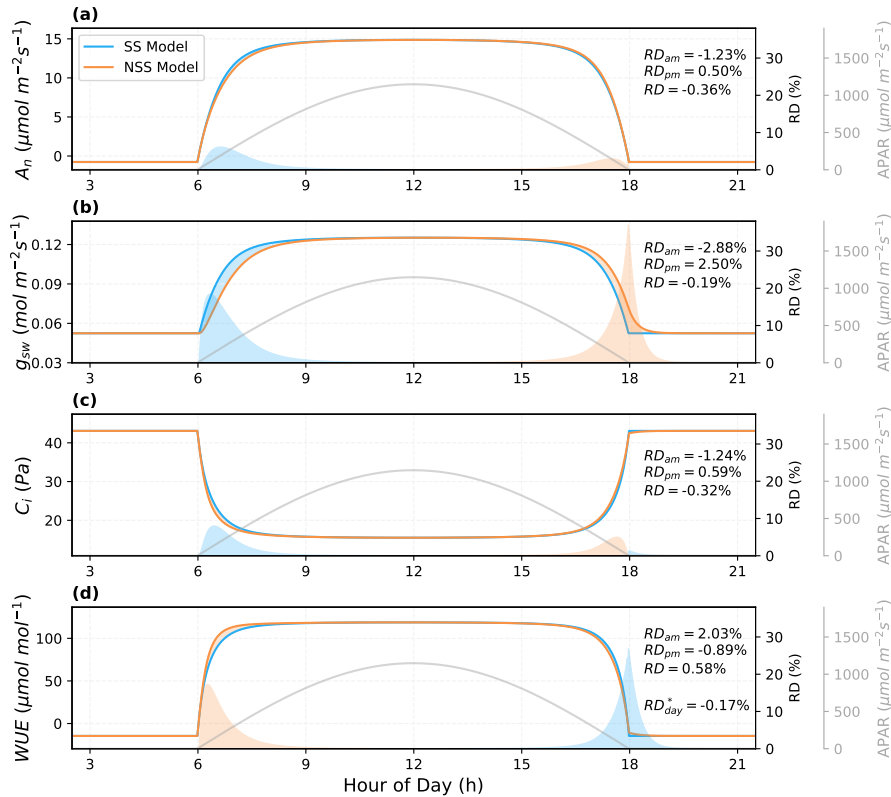
Figure 5. Predictions of the leaf diurnal course of (a) net photosynthesis rate (A_n), (b) stomatal conductance to water vapor (g_{sw}), (c) intercellular CO_2 concentration (C_i), and (d) intrinsic water-use efficiency (WUE) for a leaf with a stomatal time constant of 900 s in an ideal clear-sky day ($\tau_{op} = \tau_{cl} = 900$ s). Other environmental conditions (e.g. leaf temperature, VPD) were held constant. The shaded areas indicate the differences between the NSS and SS simulations (blue: SS > NSS; orange: SS < NSS), both in absolute and relative terms. Relative differences (RD, NSS - SS) in the temporal integrals are also presented, for morning (am, 5:00-12:00), afternoon (pm, 12:00-19:00), and daytime (5:00-19:00). RD* of WUE represents the ratio between integrated A_n and g_{sw}, differing from the RD, the integral of the instantaneous WUE during the daytime.

the major limiting factor on productivity was the decreasing light, in contrast to the sunrise where it was the available C_i
245   regulated by g_s responses that mainly constrained A_n increases. The relative differences (RDs) in integrated g_s in the morning and afternoon were both higher than those of the photosynthesis, reflecting the differences in the response speed.

The differences in predictions of A_n and g_{sw} responses also led to RDs in the intrinsic water-use efficiency (WUE, i.e. the ratio between A_n and g_{sw}). Although the mean instantaneous WUE during the daytime was higher in the NSS simulation, diurnal WUE calculated from the integrated A_n and g_{sw} was lower. This was because the gradual opening of stomata during
250   the sunrise limited assimilation in the morning, whereas during the sunset, delayed closure led to unnecessary water loss when carbon gain was constrained by low light.

3.2.2 Canopy fluxes

To quantify the impacts of the inclusion of g_s temporal response, we analyzed the simulated canopy fluxes under natural radiation variations and coupled dynamics of environmental conditions. As shown in the examples of diurnal cycle simulations (Figure 6 and 7), the SS model predicted higher variations in instantaneous fluxes in response to rapid fluctuations in radiation, particularly in transpiration rates.

When $\tau_{op} = \tau_{cl}$, the overestimate of morning g_{sw} in SS predictions was mostly compensated by an underestimate of afternoon g_{sw}, resulting in relatively minor differences in daily average g_{sw} (Figure 8c; the mean RD of daytime-mean g_{sw}, 0.5 %). However, when the time constants of stomatal opening and closure were not equal, there is overall underestimation or overestimation in both mornings and afternoons, and the daily-mean RDs can be notable (Figure 8g and k, Figure S3, Figure S4). For example, when $\tau_{op} = 3\tau_{cl}$, the faster closure than opening of stomata led to overall lower conductance over the diurnal cycles, compared to SS runs (Figure 8k; the mean RD of daytime-mean g_{sw}, -6.1 %).

In the simulations with same time constants of stomata opening and closure, the differences in fluxes between the NSS and SS predictions were not significant when integrated over monthly periods (e.g. the mean RD of transpiration in August 2017, 0.87 %, and the median, 1.0 %), but can be notable at sub-diurnal scales depending on the environmental conditions (e.g. the variation of afternoon RDs ranged from -7.4 % to 6.1 %). When there were differences in τ_{op} and τ_{cl}, the divergences between NSS and SS predictions can be more significant (e.g. when $\tau_{op} = 1/3\tau_{cl}$, the mean RD of transpiration in August 2017, 4.9 %, the maximum daily-mean RD of transpiration, 9.0 %).

The overall tendency to overestimate productivity with traditional SS models was also observed at the canopy scale, when τ_{op} was equal to or larger than τ_{cl}, as the regulation of g_s hysteresis on the supply of CO_2 for photosynthesis was not considered (Figure 8b and j). For example, in Figure 6, when rapid spikes of radiation occurred in the afternoon, the speed of g_s response constrained the increases of photosynthesis in the NSS simulation. However, when τ_{op} was smaller than τ_{cl}, predicted daily-mean photosynthesis is slightly higher in NSS simulation (Figure 8f; the mean RD of productivity in August 2017, 0.2 %). This resulted from the overall higher g_{sw}, due to faster opening than closure (Figure 8g), as higher conductance resulted in higher C_i (Figure S5), leading to generally higher rates of photosynthesis.

In contrast to the leaf-scale results, when accounting for other co-varying environmental drivers (e.g. temperature, VPD, soil water content), the SS model tended to underestimate canopy transpiration rates, when $\tau_{op} = \tau_{cl}$ (Figure 6b, Figure 7b, Figure 8a). This could be because the transpiration rates were determined by both g_{sw} and VPD. During the daytime, VPD typically increased following air temperature and peaked in the afternoon, when the slow response of stomata to the increasing VPD and decreasing radiation could result in excess water loss (Figure 7b, Figure 8 a and c). The overestimation of productivity and underestimation of transpiration in SS simulations both contributed to the overestimation of WUE. When $\tau_{op} < \tau_{cl}$, slower stomatal closure led to increased water loss and thus a more significant underestimation of transpiration in the SS predictions (Figure 8e; the mean RD of transpiration in August 2017, 4.9 %), resulting in further overestimation of the WUE. When $\tau_{op} > \tau_{cl}$, the NSS model predicted lower transpiration rates and higher WUE, compared to the SS model, because of the overall
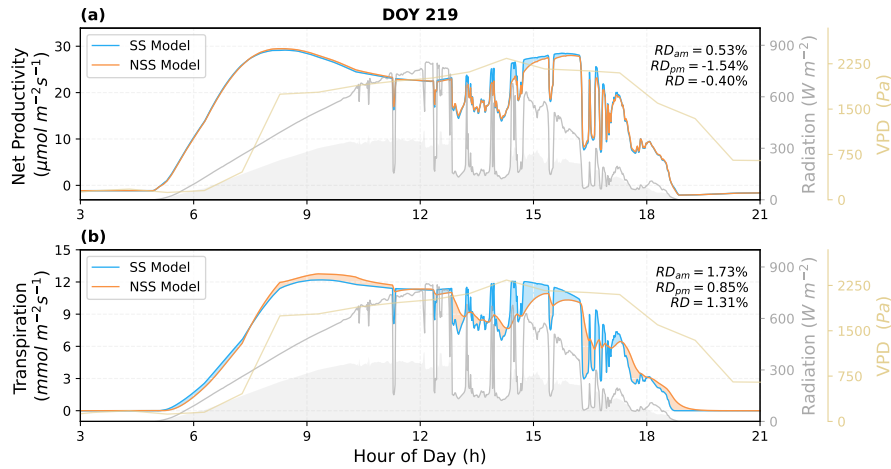
Figure 6. Comparison of the predicted diurnal cycles of ecosystem fluxes, (a) the net productivity and (b) the transpiration rate for DOY 219, 2017. The shaded areas in blue and orange indicate the differences between the NSS and SS predictions (blue: SS > NSS; orange: SS < NSS). The shaded areas in gray under the radiation curves represent the diffuse component of the total radiation. Relative differences (RD, NSS - SS) in the temporal integrated fluxes are also presented, for morning (am, 5:00-12:00), afternoon (pm, 12:00-19:00), and daytime (5:00-19:00).

lower g_{sw} (Figure 8i and k). As lower g_{sw} yielded overall lower C_i (Figure S5), larger gradients of CO_2 concentration across stomata contributed to higher WUE on daily and monthly timescales.

3.2.3 Diurnal hysteresis

To investigate the relative contributions of g_s hysteresis and environmental variables to the hysteresis observed in plant behaviors and ecosystem fluxes, we separated the effects of these two factors by comparing predicted response curves in NSS and SS simulations with and without diurnal environmental variations (e.g. temperature, VPD, soil water content). While the asymmetry of environmental variables in the diurnal cycle could lead to a modeled hysteresis of g_s in response to radiation, where g_s tended to be lower in the afternoon mainly due to higher VPD and temperature, our results (Figure 9) showed that the kinetic lag of g_s could partially offset this effect (Figure 9 b and d), even presenting an opposite tendency at low radiations. Additionally, only the NSS model simulations predicted a hysteresis of canopy transpiration, with or without the consideration of coupled environmental variations (Figure 9 g and h), in which canopy H_2O fluxes tended to be higher in the afternoon. Differences between τ_{op} and τ_{cl} affected the magnitudes of hysteresis, but the overall patterns remained similar (Figure S6, S7).
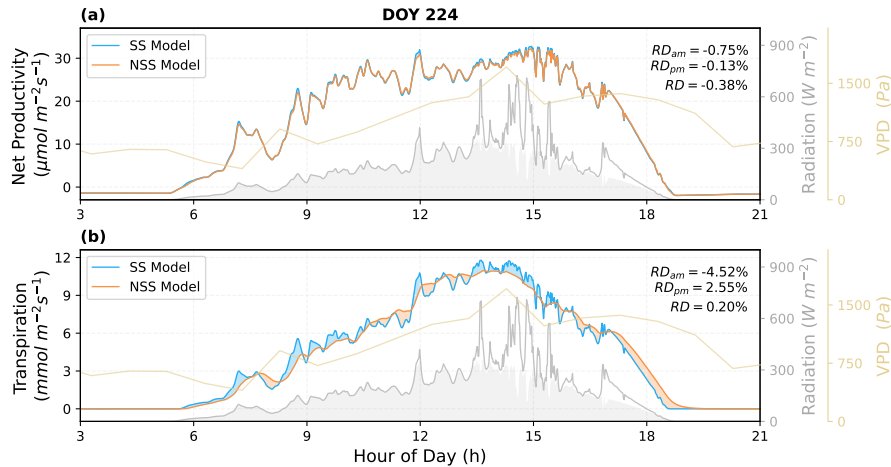
Figure 7. Comparison of the predicted diurnal cycles of ecosystem fluxes, (a) the net productivity and (b) the transpiration rate for DOY 224, 2017. The shaded areas in blue and orange indicate the differences between the NSS and SS predictions (blue: SS > NSS; orange: SS < NSS). The shaded areas in gray under the radiation curves represent the diffuse component of the total radiation. Relative differences (RD, NSS - SS) in the temporal integrated fluxes are also presented, for morning (am, 5:00-12:00), afternoon (pm, 12:00-19:00), and daytime (5:00-19:00).

3.3 Stability of the dynamic model

We further assessed the sensitivity of the dynamic modeling to the time step of simulation. Figure 10 shows the NSS model was be able to run at a time step of 10 minutes stably and still demonstrated the impacts of gradual g_s responses, as compared to the traditional practice of SS modeling at a time step of 30 minutes.

4 Discussion

In this study, we demonstrated the feasibility and benefits of implementing a non-steady-state stomatal conductance modeling framework from the leaf to canopy scale, in a new generation LSM, CliMA-Land. Our results suggested that compared to traditional steady-state models, the dynamic model was able to provide more realistic and accurate predictions of leaf temporal responses to the changes in light intensity (Section 3.1). In the meantime, modeling g_s with prognostic updates - similar to how plants control their stomata movements gradually in natural environments - neither increased computational cost nor model complexity, as simulations were simplified with iterations to solve for steady states avoided. Sun et al. (2012) pointed out the default 3-step fix-point iteration for solving the coupled $A_n - g_s$ model in CLM4 (the Community Land Model version 4) does not always converge, leading to uncertainties in flux predictions. In our simulations at the canopy scale (Section 3.3), the dynamic model could be stably run at a temporal resolution (10 min) that presented comparable efficiency to the current practice of 30-minute resolution SS simulations commonly used in LSMs (3-step prognostic updates for each SS default 3-step
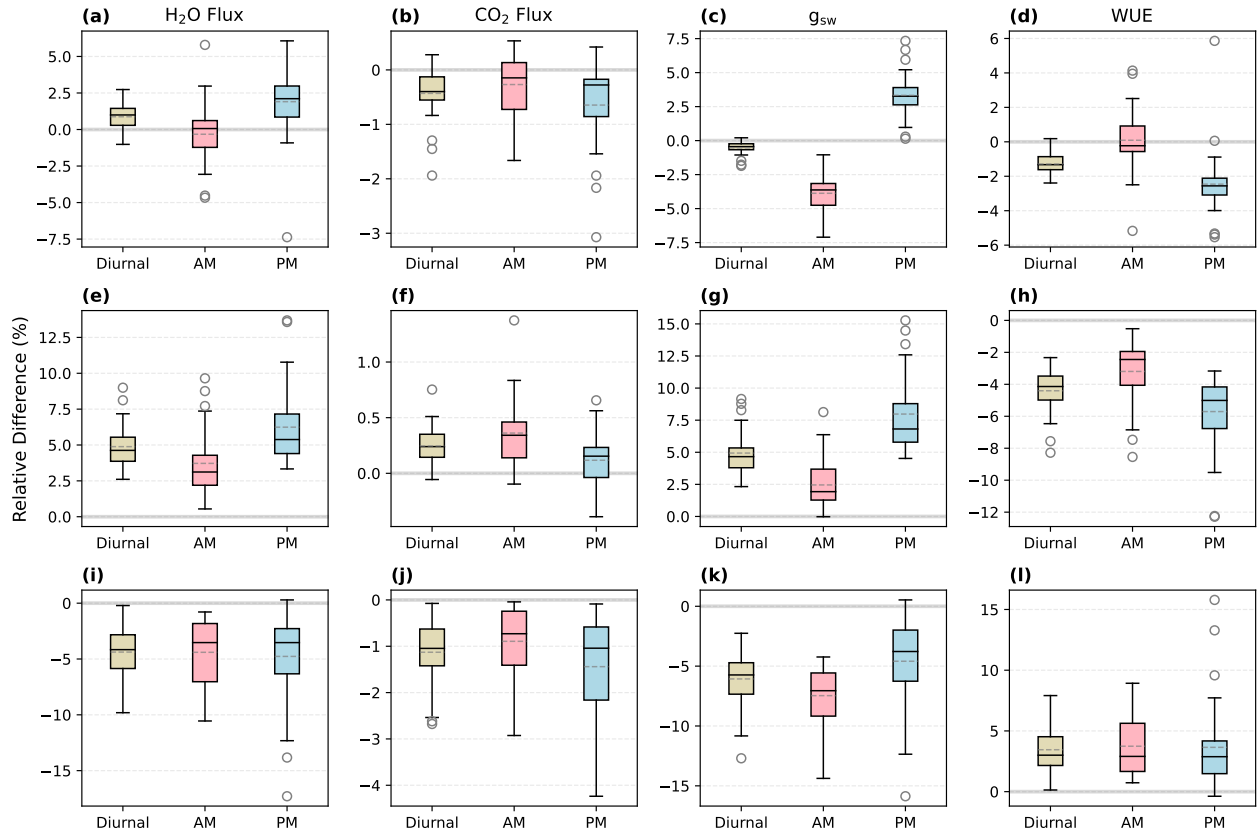
Figure 8. Relative differences (NSS - SS; RD) in the predicted daytime-mean fluxes of the NSS (time step: 1 min) and SS (1 min) simulations for August 2017. The solid line in each box indicates the median, and the dashed line represents the mean. The results for the transpiration rate (H_2O flux), net productivity (CO_2 flux), canopy-averaged stomatal conductance to water ($g$sw), and water-use efficiency (WUE) are shown in the respective columns from left to right. (a-d) $\tau_{op} = \tau_{cl} = 900\,\text{s}$, (e-h) $\tau_{op} = 300\,\text{s}$, $\tau_{cl} = 900\,\text{s}$, (i-l) $\tau_{op} = 900\,\text{s}$, $\tau_{cl} = 300\,\text{s}$. Diurnal: 5:00-19:00, AM: 5:00-12:00, PM: 12:00-19:00.

iteration). This also indicates the dynamic model can enable predictions of canopy flux dynamics at a finer time resolution with higher efficiency and accuracy.

315   With the non-steady-state model, we were able to apply a Bayesian nonlinear inversion framework to jointly fit the light response curves of both A_n and g_s, and obtain estimates for key parameters (Section 3.1). As suggested in our results (Figure 4) and previous studies (Xu and Baldocchi, 2003; Miner et al., 2017), the time step of light response curves can notably influence the estimated parameters obtained from the traditional linear fitting method for steady-state empirical models. Our framework with the dynamic model can help reduce the time required for accurate parameter estimations, particularly for leaves with long

320   time constants, as equilibrium is not required. Although the retrieval setups presented in this study may not be optimal for estimating V_{cmax}, which is typically derived from A-C_i response curves (Medlyn et al., 2002; Miao et al., 2009; Duarte et al.,

2016), a similar framework can be applied to other scenarios for estimation of various parameters, including a A-C_i curve for V_{cmax}.

Furthermore, we evaluated how the inclusion of g_s temporal responses could affect model predictions of leaf and canopy
fluxes in diurnal cycles with natural environmental variations (Section 3.2.2). The comparison of NSS and SS simulations
indicated that the differences in fluxes depended on the integration timescales, relative speed of stomatal opening and closure,
and environmental variations. In terms of instantaneous effects, slow opening of stomata tended to limit productivity responses
to rapid radiation increases, and delayed closure of g_s following decreases in radiation or increases in environmental stress
(e.g. increasing VPD) resulted in unnecessary water loss. The divergence of NSS and SS schemes was less significant when
considering the monthly integrated canopy fluxes, compared to daily or sub-diurnal scale results. The monthly differences
were more notable when the speeds of stomata opening and closure differed. The overall effects on WUE also depended
on the relative speed of opening and closure. In the simulations where stomata open at a similar or faster speed than they
close, excessive water loss in the afternoons, when VPD was high, led to a lower WUE. This also suggested that traditional
steady-state simulations may overestimate WUE. Similar impacts have been noted in studies on leaf-scale response to PPFD
fluctuations (Lawson et al., 2011; Lawson and Blatt, 2014; McAusland et al., 2016). Meanwhile, when stomata opened more
slowly than they closed, plants exhibited both a lower maximum g_s during diurnal cycles and a lower average g_s compared to
the SS runs. This resulted in reduced transpiration and increased WUE, even though productivity was also suppressed. These
results suggest that the temporal hysteresis of g_s can have impacts on integrated canopy fluxes, and further studies on variations
of stomata opening and closure speeds across plants can be helpful to assess these effects more comprehensively on larger
scales.

In addition, the hysteresis of leaf-level g_s response can contribute to the hysteresis patterns at the ecosystem scale, which
have often been solely attributed to the asymmetry of environmental variables during the daytime. For instance, higher evap-
otranspiration (ET) fluxes and sap velocity (i.e. an indicator of plant transpiration rate) have been observed in the field, with
explanation often focused on higher VPD in the afternoon following increased air temperature (Zeppel et al., 2004; Gimenez
et al., 2019; Oogathoo et al., 2020; Lin et al., 2019). Our simulations showed that the SS model with diurnal environmental
variations was unable to reproduce this hysteresis pattern, while it was captured in NSS runs. This indicated the significance
of considering g_s temporal dynamics when interpreting diurnal hysteresis in transpiration (Section 3.2.3). Moreover, observed
patterns of lower g_s in the afternoon have also been commonly explained with similar environmental asymmetry (Bai et al.,
2015; Lin et al., 2019), whilst our results suggested the kinetic lag of g_s could partially offset this effect, and thus should be
taken into account in understanding the hysteresis patterns.

Our study mainly focused on taking the first step to implement prognostic stomatal modeling in a LSM, including the impacts
on canopy flux simulations. Further improvements can be made in assessing other effects of g_s temporal responses in LSM
projections, as well as validating the comparisons with site-level observations. For example, while daily effects on canopy
productivity were minor, they may add up to significant differences in long-term vegetation growth trajectories. As plant traits
were prescribed in our simulations, the accumulative effects were not included in our analysis of the short-term predictions.
The transient limitation on photosynthesis from the slow temporal response of g_s could also cause potential photoinhibitory

damage to the photosystem II reaction centers. Future studies can focus on the parameterization of these impacts in LSMs and the evaluation of cumulative effects on plant growth and hydraulics in the long term.

The dynamic g_s model enables predictions of temporal changes in latent heat flux through transpiration in leaf energy bal-
360   ance, which allows a similar prognostic framework to be employed for the modeling of leaf temperature. Coupled dynamic modeling of stomatal conductance and leaf temperature will enhance our ability to evaluate the influences of g_s hysteresis on the feedback between leaf transpiration and thermal condition. This is out of scope of our current study but can be a valuable direction for future research efforts. Bonan et al. (2018) implemented a non-steady-state framework for leaf temperature modeling, but as steady-state g_s models were employed, iterations for stable solutions were still required. With the dynamic g_s
365   model presented in this study, the traditional nested iteration loops in leaf flux calculations, which can take up to 40 iterations to solve for a single simulation step in CLM4.5 (Bonan et al., 2018), can be replaced by more efficient and accurate prognostic updates of variables with ordinary differential equations (ODEs). Such an approach can also facilitate better couplings of LSMs with other components in Earth system models (ESMs), where ODE systems are commonly used.

5   Conclusions

370   We implemented a simplified dynamic stomatal conductance model in CliMA-Land, and evaluated its impacts on model simulations across scales. In comparison with the traditional steady-state model, the dynamic model better predicted the coupled temporal responses of A_n, g_s and C_i observed in leaf measurements. We also found uncertainties in parameter estimation for steady-state g_s models with the traditional linear fitting method, when too short of a time step used resulted in unstable estimates. We proposed an alternative approach using a Bayesian nonlinear inversion framework with a dynamic model,
375   which could help reduce the time investment for estimation, particularly for leaves with long time constants. Our results on canopy-scale simulations suggested that the effects of temporal g_s responses on ecosystem fluxes depend on the timescales of integration, relative speed of stomatal opening and closure, and environmental variations. Although the differences in monthly integrated fluxes between NSS and SS simulations were relatively minor, the hysteresis of g_s should be taken into account when predicting diurnal courses and quantifying sub-diurnal scale fluxes, as well as explaining the hysteresis patterns observed
380   in diurnal cycles. In addition, we also show that these divergences become notable when stomata open and close at different speeds.

We demonstrated that the more realistic prognostic modeling of gradual g_s response simplified the simulation as iteration loops for solving steady-states at each time step were avoided, and the dynamic model can be run at a finer time resolution that presents comparable computational costs to the current practice of steady-state leaf flux calculation. A similar framework can
385   be extended to leaf temperature modeling which will enable prognostic updates of leaf level variables with higher efficiency and accuracy, towards better couplings of LSMs with other components in Earth system models (ESMs).

Code and data availability. We coded our model and did the analysis using Julia, and the current version of the CliMA Land model with the implementation of dynamic stomatal conductance framework is available from the project website: https://github.com/CliMA/LandCliMA. Other scripts and datasets used in the study will be available in the final manuscript [to be added]

390   *Author contributions.* CF, KL and YW designed and conceptualized the study. TSM provided the leaf gas exchange measurements. YW developed CliMA Land and helped with the implementation of the dynamic model. KL performed the analysis. KL, CF and YW interpreted the results. KL composed the manuscript with contributions from all authors.

Competing interests. The contact author has declared that neither they nor their co-authors have any competing interests.

Acknowledgements. We gratefully acknowledge the financial support of the Explorer Grant of Resnick Sustainability Institute at the Califor-
395   nia Institute of Technology. TSM acknowledges funding from the NASA ECOSTRESS Science Team Project (grant no. 80NSSC20K0078)

References

Bai, Y., Zhu, G., Su, Y., Zhang, K., Han, T., Ma, J., Wang, W., Ma, T., and Feng, L.: Hysteresis loops between canopy conductance of grapevines and meteorological variables in an oasis ecosystem, Agricultural and Forest Meteorology, 214-215, 319–327, https://doi.org/10.1016/j.agrformet.2015.08.267, 2015.

Ball, J. T., Woodrow, I. E., and Berry, J. A.: A Model Predicting Stomatal Conductance and its Contribution to the Control of Photosynthesis under Different Environmental Conditions, in: Progress in Photosynthesis Research: Volume 4 Proceedings of the VIIth International Congress on Photosynthesis Providence, Rhode Island, USA, August 10–15, 1986, edited by Biggins, J., pp. 221–224, Springer Netherlands, Dordrecht, https://doi.org/10.1007/978-94-017-0519-6_48, 1987.

Berry, J. A., Beerling, D. J., and Franks, P. J.: Stomata: key players in the earth system, past and present, Current Opinion in Plant Biology, 13, 232–239, https://doi.org/10.1016/j.pbi.2010.04.013, number: 3, 2010.

Boland, J., Scott, L., and Luther, M.: Modelling the diffuse fraction of global solar radiation on a horizontal surface, Environmetrics, 12, 103–116, https://doi.org/10.1002/1099-095X(200103)12:2<103::AID-ENV447>3.0.CO;2-2, _eprint: https://onlinelibrary.wiley.com/doi/pdf/10.1002/1099-095X%28200103%2912%3A2%3C103%3A%3AAID-ENV447%3E3.0.CO%3B2-2, 2001.

Bonan, G. B., Williams, M., Fisher, R. A., and Oleson, K. W.: Modeling stomatal conductance in the earth system: linking leaf water-use efficiency and water transport along the soil–plant–atmosphere continuum, Geoscientific Model Development, 7, 2193–2222, https://doi.org/10.5194/gmd-7-2193-2014, number: 5 Publisher: Copernicus GmbH, 2014.

Bonan, G. B., Patton, E. G., Harman, I. N., Oleson, K. W., Finnigan, J. J., Lu, Y., and Burakowski, E. A.: Modeling canopy-induced turbulence in the Earth system: a unified parameterization of turbulent exchange within plant canopies and the roughness sublayer (CLM-ml v0), Geoscientific Model Development, 11, 1467–1496, https://doi.org/10.5194/gmd-11-1467-2018, number: 4 Publisher: Copernicus GmbH, 2018.

Buckley, T. N.: Modeling Stomatal Conductance, Plant Physiology, 174, 572–582, https://doi.org/10.1104/pp.16.01772, number: 2, 2017.

Butler, E. E., Datta, A., Flores-Moreno, H., Chen, M., Wythers, K. R., Fazayeli, F., Banerjee, A., Atkin, O. K., Kattge, J., Amiaud, B., Blonder, B., Boenisch, G., Bond-Lamberty, B., Brown, K. A., Byun, C., Campetella, G., Cerabolini, B. E. L., Cornelissen, J. H. C., Craine, J. M., Craven, D., de Vries, F. T., Díaz, S., Domingues, T. F., Forey, E., González-Melo, A., Gross, N., Han, W., Hattingh, W. N., Hickler, T., Jansen, S., Kramer, K., Kraft, N. J. B., Kurokawa, H., Laughlin, D. C., Meir, P., Minden, V., Niinemets, Ü., Onoda, Y., Peñuelas, J., Read, Q., Sack, L., Schamp, B., Soudzilovskaia, N. A., Spasojevic, M. J., Sosinski, E., Thornton, P. E., Valladares, F., van Bodegom, P. M., Williams, M., Wirth, C., and Reich, P. B.: Mapping local and global variability in plant trait distributions, Proceedings of the National Academy of Sciences, 114, E10 937–E10 946, https://doi.org/10.1073/pnas.1708984114, publisher: Proceedings of the National Academy of Sciences, 2017.

Collatz, G. J., Ball, J. T., Grivet, C., and Berry, J. A.: Physiological and environmental regulation of stomatal conductance, photosynthesis and transpiration: a model that includes a laminar boundary layer, Agricultural and Forest Meteorology, 54, 107–136, https://doi.org/10.1016/0168-1923(91)90002-8, 1991.

Croft, H., Chen, J. M., Wang, R., Mo, G., Luo, S., Luo, X., He, L., Gonsamo, A., Arabian, J., and Zhang, Y.: The global distribution of leaf chlorophyll content, Remote Sensing of Environment, 236, 111 479, iSBN: 0034-4257 Publisher: Elsevier, 2020.

Damour, G., Simonneau, T., Cochard, H., and Urban, L.: An overview of models of stomatal conductance at the leaf level, Plant, Cell & Environment, 33, 1419–1438, https://doi.org/10.1111/j.1365-3040.2010.02181.x, number: 9 _eprint: https://onlinelibrary.wiley.com/doi/pdf/10.1111/j.1365-3040.2010.02181.x, 2010.

De Kauwe, M. G., Kala, J., Lin, Y.-S., Pitman, A. J., Medlyn, B. E., Duursma, R. A., Abramowitz, G., Wang, Y.-P., and Miralles, D. G.: A test of an optimal stomatal conductance scheme within the CABLE land surface model, Geoscientific Model Development, 8, 431–452, https://doi.org/10.5194/gmd-8-431-2015, publisher: Copernicus GmbH, 2015.

Duarte, A., Katata, G., Hoshika, Y., Hossain, M., Kreuzwieser, J., Arneth, A., and Ruehr, N.: Immediate and potential long-term effects of consecutive heat waves on the photosynthetic performance and water balance in Douglas-fir, Journal of Plant Physiology, 2016.

Durand, M., Murchie, E. H., Lindfors, A. V., Urban, O., Aphalo, P. J., and Robson, T. M.: Diffuse solar radiation and canopy photosynthesis in a changing environment, Agricultural and Forest Meteorology, 311, 108 684, https://doi.org/10.1016/j.agrformet.2021.108684, 2021.

Dutta, D., Schimel, D. S., Sun, Y., van der Tol, C., and Frankenberg, C.: Optimal inverse estimation of ecosystem parameters from observations of carbon and energy fluxes, Biogeosciences, 16, 77–103, https://doi.org/10.5194/bg-16-77-2019, number: 1 Publisher: Copernicus GmbH, 2019.

Farquhar, G. D., von Caemmerer, S., and Berry, J. A.: A biochemical model of photosynthetic CO2 assimilation in leaves of C 3 species, Planta, 149, 78–90, https://doi.org/10.1007/BF00386231, number: 1, 1980.

Gimenez, B. O., Jardine, K. J., Higuchi, N., Negrón-Juárez, R. I., Sampaio-Filho, I. d. J., Cobello, L. O., Fontes, C. G., Dawson, T. E., Varadharajan, C., Christianson, D. S., Spanner, G. C., Araújo, A. C., Warren, J. M., Newman, B. D., Holm, J. A., Koven, C. D., McDowell, N. G., and Chambers, J. Q.: Species-Specific Shifts in Diurnal Sap Velocity Dynamics and Hysteretic Behavior of Ecophysiological Variables During the 2015–2016 El Niño Event in the Amazon Forest, Frontiers in Plant Science, 10, https://www.frontiersin.org/articles/10.3389/fpls.2019.00830, 2019.

He, L., Chen, J. M., Pisek, J., Schaaf, C. B., and Strahler, A. H.: Global clumping index map derived from the MODIS BRDF product, Remote Sensing of Environment, 119, 118–130, https://doi.org/10.1016/j.rse.2011.12.008, 2012.

Hersbach, H., Bell, B., Berrisford, P., Biavati, G., Horányi, A., Muñoz Sabater, J., Nicolas, J., Peubey, C., Radu, R., Rozum, I., et al.: ERA5 hourly data on single levels from 1979 to present, Copernicus climate change service (c3s) climate data store (cds), 10, 2018.

Kaiser, H. and Kappen, L.: In situ observation of stomatal movements and gas exchange of Aegopodium podagraria L. in the understorey, Journal of Experimental Botany, 51, 1741–1749, https://doi.org/10.1093/jexbot/51.351.1741, 2000.

Kirschbaum, M. U. F., Gross, L. J., and Pearcy, R. W.: Observed and modelled stomatal responses to dynamic light environments in the shade plant Alocasia macrorrhiza, Plant, Cell & Environment, 11, 111–121, https://doi.org/10.1111/1365-3040.ep11604898, _eprint: https://onlinelibrary.wiley.com/doi/pdf/10.1111/1365-3040.ep11604898, 1988.

Lawson, T. and Blatt, M. R.: Stomatal Size, Speed, and Responsiveness Impact on Photosynthesis and Water Use Efficiency, Plant Physiology, 164, 1556–1570, https://doi.org/10.1104/pp.114.237107, number: 4 Publisher: American Society of Plant Biologists Section: TOPICAL REVIEWS - FOCUS, 2014.

Lawson, T., von Caemmerer, S., and Baroli, I.: Photosynthesis and Stomatal Behaviour, in: Progress in Botany 72, edited by Lüttge, U. E., Beyschlag, W., Büdel, B., and Francis, D., Progress in Botany, pp. 265–304, Springer, Berlin, Heidelberg, https://doi.org/10.1007/978-3-642-13145-5_11, 2011.

Leuning, R.: Modelling Stomatal Behaviour and and Photosynthesis of Eucalyptus grandis, Functional Plant Biology, 17, 159, https://doi.org/10.1071/PP9900159, 1990.

Leuning, R.: A critical appraisal of a combined stomatal-photosynthesis model for C3 plants, Plant, Cell & Environment, 18, 339–355, https://doi.org/10.1111/j.1365-3040.1995.tb00370.x, _eprint: https://onlinelibrary.wiley.com/doi/pdf/10.1111/j.1365-3040.1995.tb00370.x, 1995.

Levenberg, K.: A method for the solution of certain non-linear problems in least squares, Quarterly of Applied Mathematics, 2, 164–168, https://doi.org/10.1090/qam/10666, 1944.

Lin, C., Gentine, P., Frankenberg, C., Zhou, S., Kennedy, D., and Li, X.: Evaluation and mechanism exploration of the diurnal hysteresis of ecosystem fluxes, Agricultural and Forest Meteorology, 278, 107 642, https://doi.org/10.1016/j.agrformet.2019.107642, 2019.

Liozon, R., Badeck, F.-W., Genty, B., Meyer, S., and Saugier, B.: Leaf photosynthetic characteristics of beech (Fagus sylvatica) saplings during three years of exposure to elevated CO(2) concentration, Tree Physiology, 20, 239–247, https://doi.org/10.1093/treephys/20.4.239, 2000.

Luo, X., Keenan, T. F., Chen, J. M., Croft, H., Colin Prentice, I., Smith, N. G., Walker, A. P., Wang, H., Wang, R., Xu, C., and Zhang, Y.: Global variation in the fraction of leaf nitrogen allocated to photosynthesis, Nature Communications, 12, 4866, https://doi.org/10.1038/s41467-021-25163-9, number: 1 Publisher: Nature Publishing Group, 2021.

Marquardt, D. W.: An Algorithm for Least-Squares Estimation of Nonlinear Parameters, Journal of the Society for Industrial and Applied Mathematics, 11, 431–441, https://doi.org/10.1137/0111030, publisher: Society for Industrial and Applied Mathematics, 1963.

Martins, S. C. V., McAdam, S. A. M., Deans, R. M., DaMatta, F. M., and Brodribb, T. J.: Stomatal dynamics are limited by leaf hydraulics in ferns and conifers: results from simultaneous measurements of liquid and vapour fluxes in leaves, Plant, Cell & Environment, 39, 694–705, https://doi.org/10.1111/pce.12668, _eprint: https://onlinelibrary.wiley.com/doi/pdf/10.1111/pce.12668, 2016.

Matthews, J. S., Vialet-Chabrand, S., and Lawson, T.: Acclimation to Fluctuating Light Impacts the Rapidity of Response and Diurnal Rhythm of Stomatal Conductance, Plant Physiology, 176, 1939–1951, https://doi.org/10.1104/pp.17.01809, 2018.

McAusland, L., Vialet-Chabrand, S., Davey, P., Baker, N. R., Brendel, O., and Lawson, T.: Effects of kinetics of light-induced stomatal responses on photosynthesis and water-use efficiency, New Phytologist, 211, 1209–1220, https://doi.org/10.1111/nph.14000, _eprint: https://onlinelibrary.wiley.com/doi/pdf/10.1111/nph.14000, 2016.

Medlyn, B. E., Dreyer, E., Ellsworth, D., Forstreuter, M., Harley, P. C., Kirschbaum, M. U. F., Le Roux, X., Montpied, P., Strassemeyer, J., Walcroft, A., Wang, K., and Loustau, D.: Temperature response of parameters of a biochemically based model of photosynthesis. II. A review of experimental data, Plant, Cell & Environment, 25, 1167–1179, https://doi.org/10.1046/j.1365-3040.2002.00891.x, _eprint: https://onlinelibrary.wiley.com/doi/pdf/10.1046/j.1365-3040.2002.00891.x, 2002.

Medlyn, B. E., Duursma, R. A., Eamus, D., Ellsworth, D. S., Prentice, I. C., Barton, C. V. M., Crous, K. Y., De Angelis, P., Freeman, M., and Wingate, L.: Reconciling the optimal and empirical approaches to modelling stomatal conductance, Global Change Biology, 17, 2134–2144, https://doi.org/10.1111/j.1365-2486.2010.02375.x, _eprint: https://onlinelibrary.wiley.com/doi/pdf/10.1111/j.1365-2486.2010.02375.x, 2011.

Meeker, E. W., Magney, T. S., Bambach, N., Momayyezi, M., and McElrone, A. J.: Modification of a gas exchange system to measure active and passive chlorophyll fluorescence simultaneously under field conditions, AoB PLANTS, 13, plaa066, https://doi.org/10.1093/aobpla/plaa066, 2021.

Miao, Z., Xu, M., Lathrop Jr., R. G., and Wang, Y.: Comparison of the A–Cc curve fitting methods in determining maximum ribulose 1·5-bisphosphate carboxylase/oxygenase carboxylation rate, potential light saturated electron transport rate and leaf dark respiration, Plant, Cell & Environment, 32, 109–122, https://doi.org/10.1111/j.1365-3040.2008.01900.x, _eprint: https://onlinelibrary.wiley.com/doi/pdf/10.1111/j.1365-3040.2008.01900.x, 2009.

Miner, G. L., Bauerle, W. L., and Baldocchi, D. D.: Estimating the sensitivity of stomatal conductance to photosynthesis: a review, Plant, Cell & Environment, 40, 1214–1238, https://doi.org/10.1111/pce.12871, _eprint: https://onlinelibrary.wiley.com/doi/pdf/10.1111/pce.12871, 2017.

Naumburg, E. and Ellsworth, D. S.: Photosynthetic sunfleck utilization potential of understory saplings growing under elevated CO2 in FACE, Oecologia, 122, 163–174, https://doi.org/10.1007/PL00008844, 2000.

Noe, S. M. and Giersch, C.: A simple dynamic model of photosynthesis in oak leaves: coupling leaf conductance and photosynthetic carbon fixation by a variable intracellular CO2 pool, Functional plant biology: FPB, 31, 1195–1204, https://doi.org/10.1071/FP03251, 2004.

Oogathoo, S., Houle, D., Duchesne, L., and Kneeshaw, D.: Vapour pressure deficit and solar radiation are the major drivers of transpiration of balsam fir and black spruce tree species in humid boreal regions, even during a short-term drought, Agricultural and Forest Meteorology, 291, 108 063, https://doi.org/10.1016/j.agrformet.2020.108063, 2020.

Ozeki, K., Miyazawa, Y., and Sugiura, D.: Rapid stomatal closure contributes to higher water use efficiency in major C4 compared to C3 Poaceae crops, Plant Physiology, 189, 188–203, https://doi.org/10.1093/plphys/kiac040, 2022.

Pearcy, R. W. and Seemann, J. R.: Photosynthetic Induction State of Leaves in a Soybean Canopy in Relation to Light Regulation of Ribulose-1-5-Bisphosphate Carboxylase and Stomatal Conductance 1, Plant Physiology, 94, 628–633, https://doi.org/10.1104/pp.94.2.628, 1990.

Rayment, M. B., Loustau, D., and Jarvis, P. G.: Measuring and modeling conductances of black spruce at three organizational scales: shoot, branch and canopy, Tree Physiology, 20, 713–723, https://doi.org/10.1093/treephys/20.11.713, 2000.

Rodgers, C. D.: Inverse Methods For Atmospheric Sounding: Theory And Practice, World Scientific, google-Books-ID: Xv7sCgAAQBAJ, 2000.

Sperry, J. S., Adler, F. R., Campbell, G. S., and Comstock, J. P.: Limitation of plant water use by rhizosphere and xylem conductance: results from a model, Plant, Cell & Environment, 21, 347–359, https://doi.org/10.1046/j.1365-3040.1998.00287.x, _eprint: https://onlinelibrary.wiley.com/doi/pdf/10.1046/j.1365-3040.1998.00287.x, 1998.

Sperry, J. S., Hacke, U. G., Oren, R., and Comstock, J. P.: Water deficits and hydraulic limits to leaf water supply, Plant, Cell & Environment, 25, 251–263, https://doi.org/10.1046/j.0016-8025.2001.00799.x, _eprint: https://onlinelibrary.wiley.com/doi/pdf/10.1046/j.0016-8025.2001.00799.x, 2002.

Sun, Y., Gu, L., and Dickinson, R. E.: A numerical issue in calculating the coupled carbon and water fluxes in a climate model, Journal of Geophysical Research: Atmospheres, 117, https://doi.org/10.1029/2012JD018059, number: D22 _eprint: https://onlinelibrary.wiley.com/doi/pdf/10.1029/2012JD018059, 2012.

Sun, Y., Gu, L., Dickinson, R. E., Norby, R. J., Pallardy, S. G., and Hoffman, F. M.: Impact of mesophyll diffusion on estimated global land CO2 fertilization, Proceedings of the National Academy of Sciences, 111, 15 774–15 779, https://doi.org/10.1073/pnas.1418075111, publisher: Proceedings of the National Academy of Sciences, 2014.

Venturas, M. D., Sperry, J. S., Love, D. M., Frehner, E. H., Allred, M. G., Wang, Y., and Anderegg, W. R. L.: A stomatal control model based on optimization of carbon gain versus hydraulic risk predicts aspen sapling responses to drought, New Phytologist, 220, 836–850, https://doi.org/10.1111/nph.15333, number: 3, 2018.

Vialet-Chabrand, S., Matthews, J. S. A., Brendel, O., Blatt, M. R., Wang, Y., Hills, A., Griffiths, H., Rogers, S., and Lawson, T.: Modelling water use efficiency in a dynamic environment: An example using Arabidopsis thaliana, Plant Science, 251, 65–74, https://doi.org/10.1016/j.plantsci.2016.06.016, 2016.

Vialet-Chabrand, S. R., Matthews, J. S., McAusland, L., Blatt, M. R., Griffiths, H., and Lawson, T.: Temporal Dynamics of Stomatal Behavior: Modeling and Implications for Photosynthesis and Water Use1[OPEN], Plant Physiology, 174, 603–613, https://doi.org/10.1104/pp.17.00125, number: 2, 2017.

545 Vialet-Chabrand, S., Dreyer, E., and Brendel, O.: Performance of a new dynamic model for predicting diurnal time courses of stomatal conductance at the leaf level, Plant, Cell & Environment, 36, 1529–1546, https://doi.org/https://doi.org/10.1111/pce.12086, number: 8 _eprint: https://onlinelibrary.wiley.com/doi/pdf/10.1111/pce.12086, 2013.

Vico, G., Manzoni, S., Palmroth, S., and Katul, G.: Effects of stomatal delays on the economics of leaf gas exchange under intermittent light regimes, New Phytologist, 192, 640–652, https://doi.org/10.1111/j.1469-8137.2011.03847.x, _eprint:
550 https://onlinelibrary.wiley.com/doi/pdf/10.1111/j.1469-8137.2011.03847.x, 2011.

Wang, Y. and Frankenberg, C.: On the impact of canopy model complexity on simulated carbon, water, and solar-induced chlorophyll fluorescence fluxes, Biogeosciences, 19, 29–45, https://doi.org/10.5194/bg-19-29-2022, publisher: Copernicus GmbH, 2022.

Wang, Y., Sperry, J. S., Anderegg, W. R. L., Venturas, M. D., and Trugman, A. T.: A theoretical and empirical assessment of stomatal optimization modeling, New Phytologist, 227, 311–325, https://doi.org/10.1111/nph.16572, number: 2, 2020.

555 Wang, Y., Köhler, P., He, L., Doughty, R., Braghiere, R. K., Wood, J. D., and Frankenberg, C.: Testing stomatal models at the stand level in deciduous angiosperm and evergreen gymnosperm forests using CliMA Land (v0.1), Geoscientific Model Development, 14, 6741–6763, https://doi.org/10.5194/gmd-14-6741-2021, publisher: Copernicus GmbH, 2021.

Wang, Y., Köhler, P., Braghiere, R. K., Longo, M., Doughty, R., Bloom, A. A., and Frankenberg, C.: GriddingMachine, a database and software for Earth system modeling at global and regional scales, Scientific Data, 9, 258, https://doi.org/10.1038/s41597-022-01346-x,
560 number: 1 Publisher: Nature Publishing Group, 2022.

Wang, Y., Braghiere, R. K., Longo, M., Norton, A. J., Köhler, P., Doughty, R., Yin, Y., Bloom, A. A., and Frankenberg, C.: Modeling Global Vegetation Gross Primary Productivity, Transpiration and Hyperspectral Canopy Radiative Transfer Simultaneously Using a Next Generation Land Surface Model—CliMA Land, Journal of Advances in Modeling Earth Systems, 15, e2021MS002 964, https://doi.org/10.1029/2021MS002964, _eprint: https://onlinelibrary.wiley.com/doi/pdf/10.1029/2021MS002964, 2023.

565 Wolf, A., Anderegg, W. R. L., and Pacala, S. W.: Optimal stomatal behavior with competition for water and risk of hydraulic impairment, Proceedings of the National Academy of Sciences, 113, E7222–E7230, https://doi.org/10.1073/pnas.1615144113, publisher: Proceedings of the National Academy of Sciences, 2016.

Xu, L. and Baldocchi, D. D.: Seasonal trends in photosynthetic parameters and stomatal conductance of blue oak (Quercus douglasii) under prolonged summer drought and high temperature, Tree Physiology, 23, 865–877, https://doi.org/10.1093/treephys/23.13.865, number: 13,
570 2003.

Yuan, H., Dai, Y., Xiao, Z., Ji, D., and Shangguan, W.: Reprocessing the MODIS Leaf Area Index products for land surface and climate modelling, Remote Sensing of Environment, 115, 1171–1187, https://doi.org/10.1016/j.rse.2011.01.001, 2011.

Zeppel, M. J. B., Murray, B. R., Barton, C., and Eamus, D.: Seasonal responses of xylem sap velocity to VPD and solar radiation during drought in a stand of native trees in temperate Australia, Functional Plant Biology, 31, 461, https://doi.org/10.1071/FP03220, 2004.
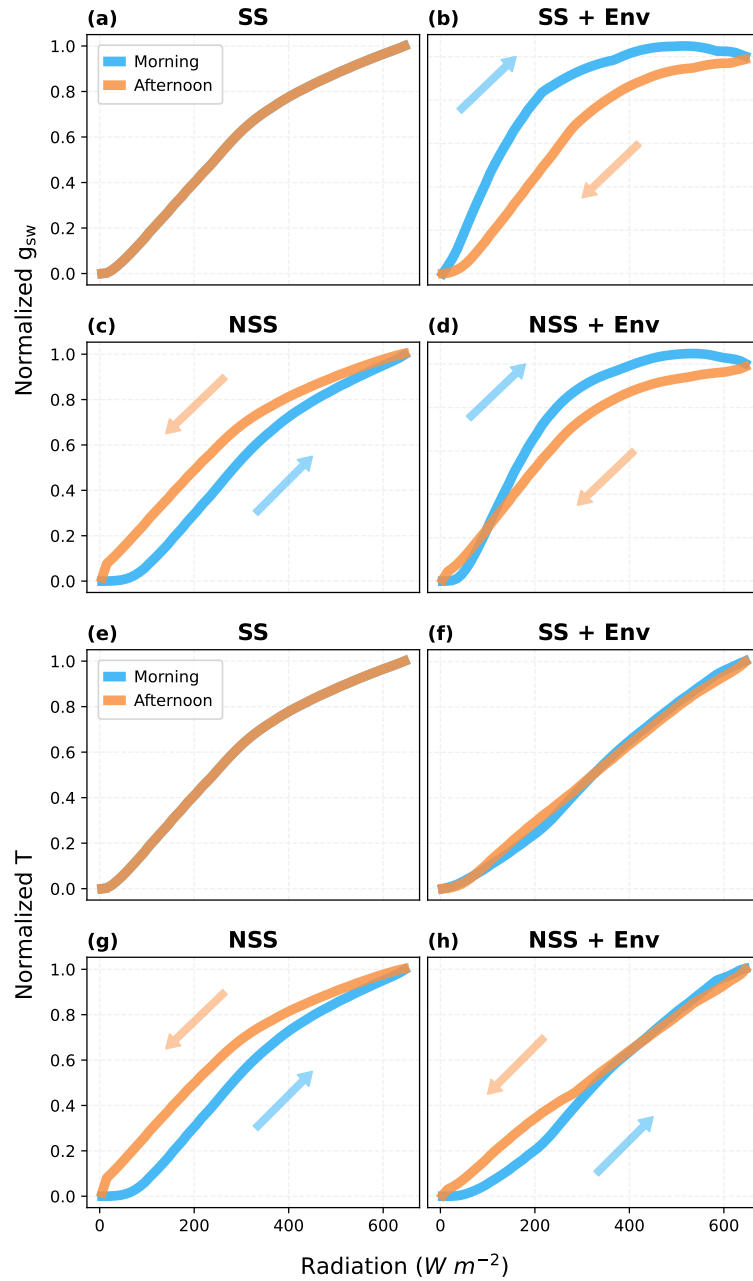
Figure 9. Hysteresis of the canopy-mean stomatal conductance (g_{sw}) and canopy transpiration rate (T) in response to radiation during an ideal clear-sky day, when $\tau_{op} = \tau_{cl} = 900\,\text{s}$. (a, e) SS model, (b, f) SS model with coupled diurnal variations of environmental conditions (Env, e.g. air temperature, VPD), (c, g) NSS model, (d, h) NSS model with Env. (a-d) normalized g_{sw} responses, (e-h) normalized T responses. In simulations without Env variations, except for the radiation, all the other environmental drivers were kept at the daytime means. g_{sw} and T is normalized with the values at noon (12:00). Arrows indicate the increasing and decreasing parts of the diurnal courses.
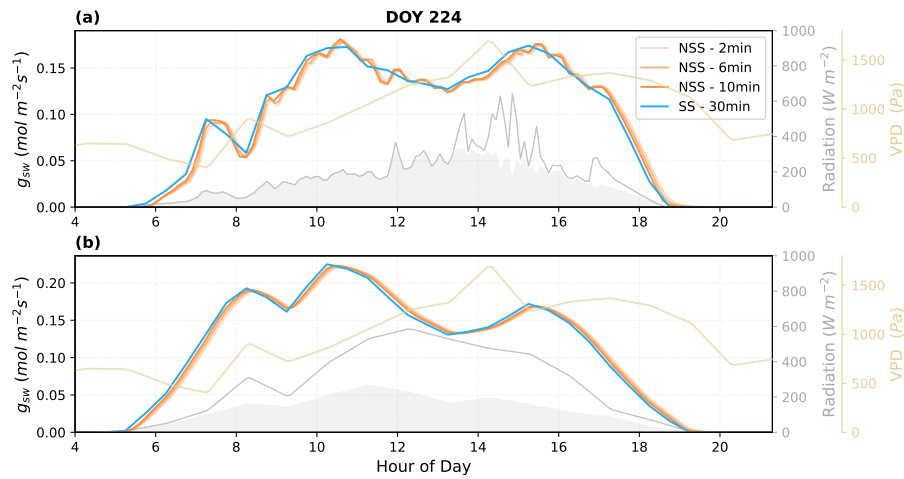
Figure 10. Simulations of dynamic g_{sw} using different time steps (2 min, 6 min, 10 min) and comparison with the traditional steady-state modeling (30-minute resolution) predictions. a) using high temporal-resolution PAR as radiation input, values are resampled accordingly to match the time step used; b) using ERA5 hourly radiation as input, values are linearly interpolated to 30-minute resolution. The shaded areas in gray under the radiation curves represent the diffuse component of the total radiation.

S1 Supplementary Information Text

S1.1 Climate Modeling Alliance (CliMA) Land Configuration

In this study, we mainly employed the soil-plant-air continuum (SPAC) module of CliMA Land (github.com /CliMA/Land) to run simulations with different stomatal modeling frameworks. The SPAC module consists of four key sub-modules: canopy radiative transfer (RT), plant hydraulics, photosynthesis, and stomatal models (Figure S1). At each time-step, the SPAC module first calls the canopy RT module to compute the radiation condition for each canopy layer and leaf angle group, then it uses the photosynthesis, plantHydraulics and stomatal models modules to calculate the leaf-level stomatal conductance and photosynthesis rates, based on which it computes the canopy fluxes (Wang et al., 2023).

For the canopy RT, we employed a vertically layered canopy scheme with leaf angular distribution and a hyperspectral radiation transfer scheme (adapted from the Soil Canopy Observation of Photosynthesis and Energy fluxes model (SCOPE); (van der Tol et al., 2009; Yang et al., 2017)). For the photosynthesis module, we used the classic photosynthesis model developed by Farquhar et al. (1980) for C3 plants. For the stomatal models, due to the limited availability of hydraulic traits data in the test region, we applied a tuning factor based on soil water potential rather than plant hydraulics to g_1 to account for the response of stomata to water supply. The boundary layer conductance to water (g_{bw}) of leaf level predictions were prescribed using the estimated g_{bw} provided in LI6800 measurements. The g_{bw} in canopy scale simulations was assumed to be a constant at $3\,\mathrm{mol\,m^{-2}\,s^{-1}}$, which is a relatively high conductance to make sure that the boundary layer conductance is not the main limiting factor of CO_2 supply (as our focus is on effects from stomatal conductance). We acknowledge more realistic g_{bw} values including calculation from wind speed and leaf width, which requires vertically resolved heterogeneous micro-climates and is under development.

In the steady-state mode, we ran iterations of the SPAC functions to find the stable solution for the given conditions at each time-step. In the prognostic mode, the simplified stomatal model was solved using the Euler method with a fixed step size, which is the time ~~steps~~ step used in each simulation. As current LSMs commonly use a time-step of 30 min or 60 min, we tested the stability of our model on 2, 6, and 10 min resolution for efficiency comparison, besides the fine 1 min resolution for flux comparison. We also tested that our method provides similar results with a much finer time step (1s, 1/60 of the 1min time step used for the comparison), the relative difference is minimal, 0.2 ± 0.1 %, indicating the time step we chose is sufficient for our simulations and comparison.

Vegetation traits and properties, including leaf chlorophyll content, leaf mass per area, leaf photosynthetic capacity, stomatal model g_1, Leaf area index, clumping index were prescribed for the test region, extracted from the global datasets (Croft et al., 2020; Butler et al., 2017; Luo et al., 2021; De Kauwe et al., 2015; Yuan et al., 2011; He et al., 2012). In this study, CliMA Land simulations were conducted offline. Environmental drivers (e.g. air temperature, dew-point temperature, volumetric soil water, wind speed etc.) were extracted from ERA5 reanalysis datasets (Hersbach et al., 2018) and updated accordingly at each step.

S2   Supplementary Figures
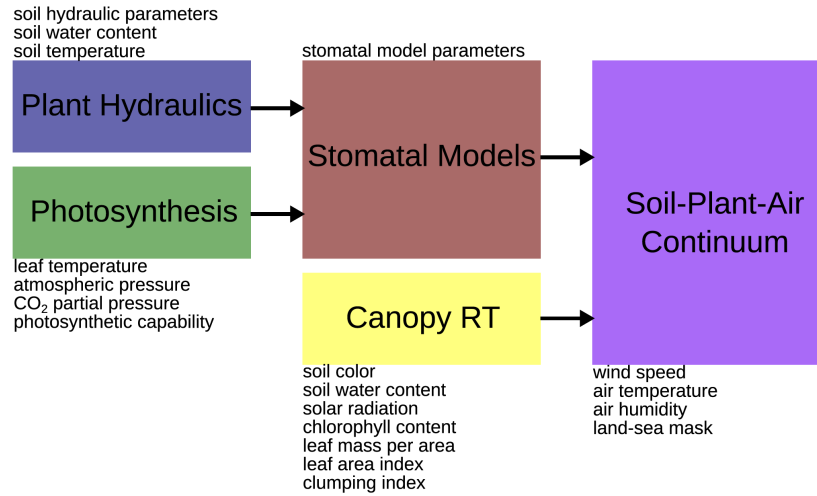
Figure S1: Model hierarchy of soil-plant-air continuum (SPAC) module of CliMA Land (from Wang et al. (2023)). Black arrows indicate the dependencies within the SPAC module, and the text next to each box describes the main parameters and weather drivers used in CliMA Land.
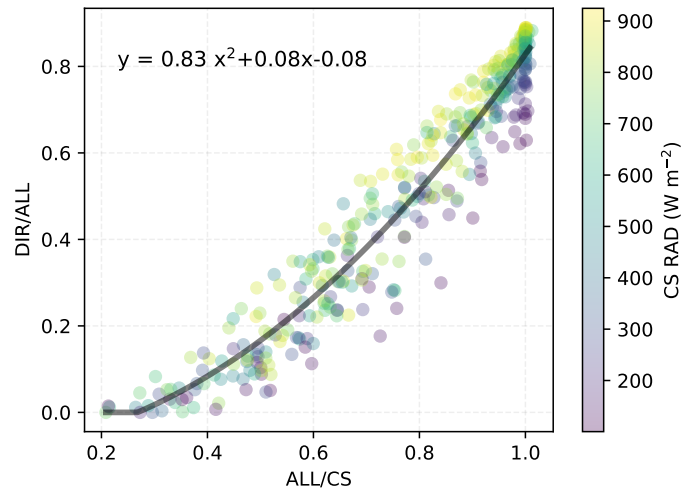
Figure S2: The empirical relationship between the direct radiation (DIR) fraction and the ratio between the total downward solar radiation (ALL) and the clear sky radiation (CS) in August 2017, filtered by 100 W m^{-2} CS radiation. Radiations are from the ERA5-Land hourly dataset.
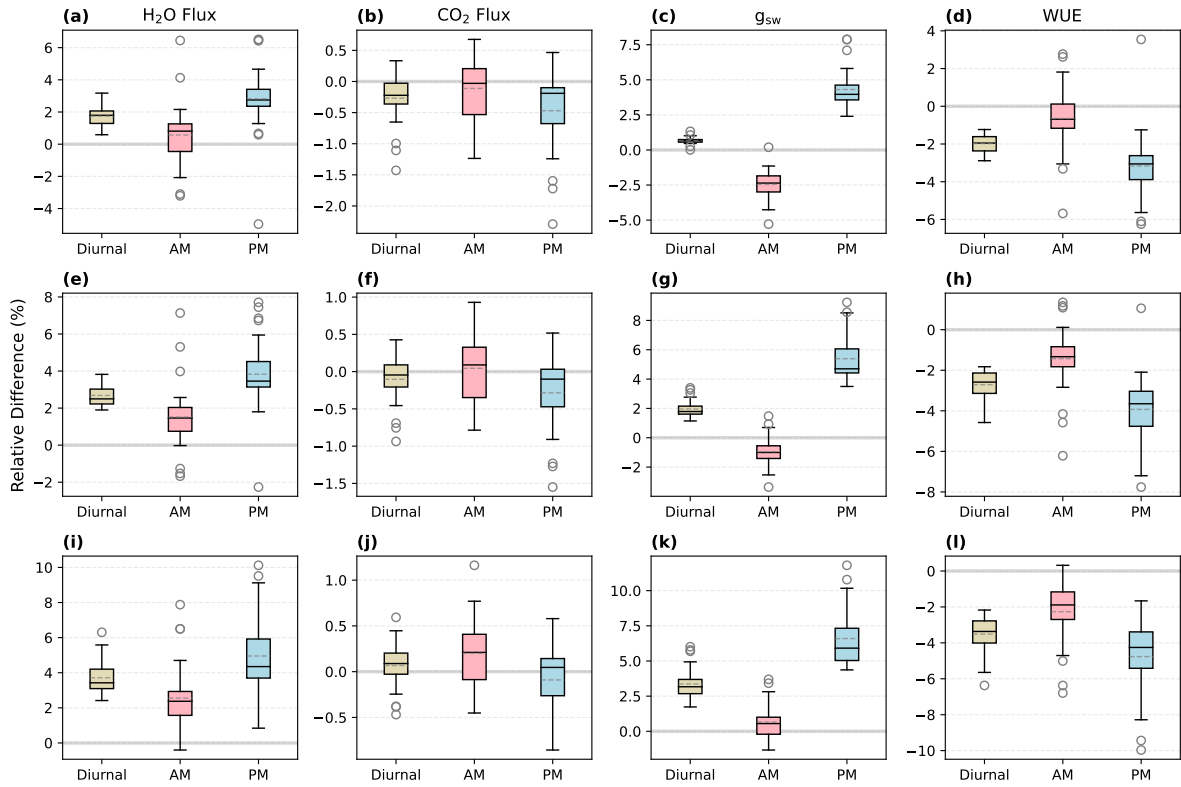
Figure S3: Relative differences (NSS - SS; RD) in the predicted daytime-mean fluxes of the NSS and SS simulations for August 2017, for results when $\tau_{op}/\tau_{cl} < 1$. The solid line in each box indicates the median, and the dashed line represents the mean. The results for the transpiration rate (H_2O flux), net productivity (CO_2 flux), canopy-averaged stomatal conductance to water (g_{sw}), and water-use efficiency (WUE) are shown in the respective columns from left to right. (a-d) $\tau_{op} = 750\,\mathrm{s}$, $\tau_{cl} = 900\,\mathrm{s}$, (e-h) $\tau_{op} = 600\,\mathrm{s}$, $\tau_{cl} = 900\,\mathrm{s}$, (i-l) $\tau_{op} = 450\,\mathrm{s}$, $\tau_{cl} = 900\,\mathrm{s}$. Diurnal: 5:00-19:00, AM: 5:00-12:00, PM: 12:00-19:00.
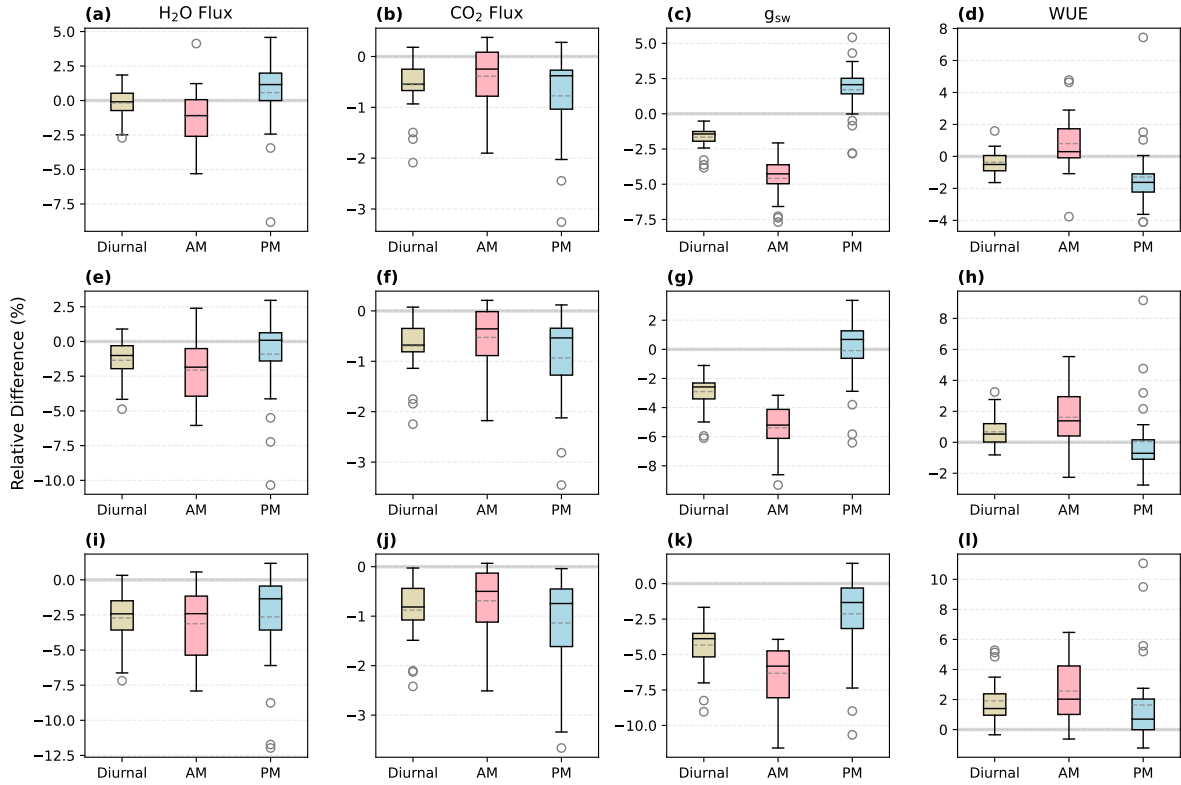
Figure S4: Relative differences (NSS - SS; RD) in the predicted daytime-mean fluxes of the NSS and SS simulations for August 2017, for results when $\tau_{op}/\tau_{cl} > 1$. The solid line in each box indicates the median, and the dashed line represents the mean. The results for the transpiration rate (H_2O flux), net productivity (CO_2 flux), canopy-averaged stomatal conductance to water (g_{sw}), and water-use efficiency (WUE) are shown in the respective columns from left to right. (a-d) $\tau_{op} = 900\,s$, $\tau_{cl} = 750\,s$, (e-h) $\tau_{op} = 900\,s$, $\tau_{cl} = 600\,s$, (i-l) $\tau_{op} = 900\,s$, $\tau_{cl} = 450\,s$. Diurnal: 5:00-19:00, AM: 5:00-12:00, PM: 12:00-19:00.
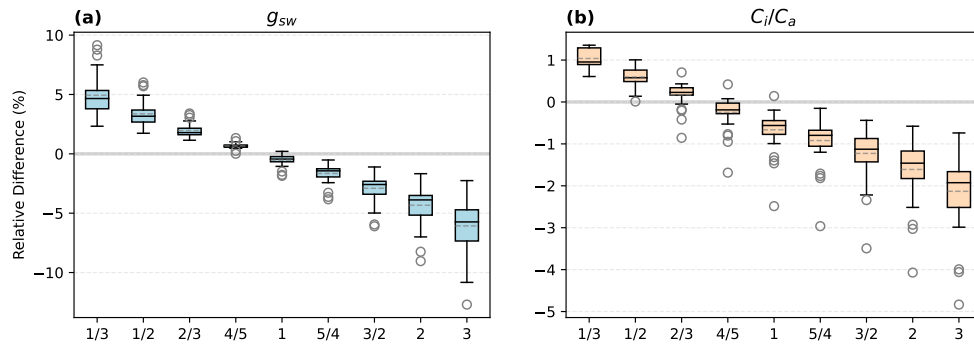
Figure S5: Relative differences (NSS - SS; RD) in the predicted daytime-mean (5:00-19:00) (a) canopy-averaged stomatal conductance to water (g_{sw}) and (b) intercelluar CO_2 concentration (Ci). The solid line in each box indicates the median, and the dashed line represents the mean. Labels on the x-axis indicate the ratio between τ_{op} and τ_{cl}, with the larger one kept as $900\,s$
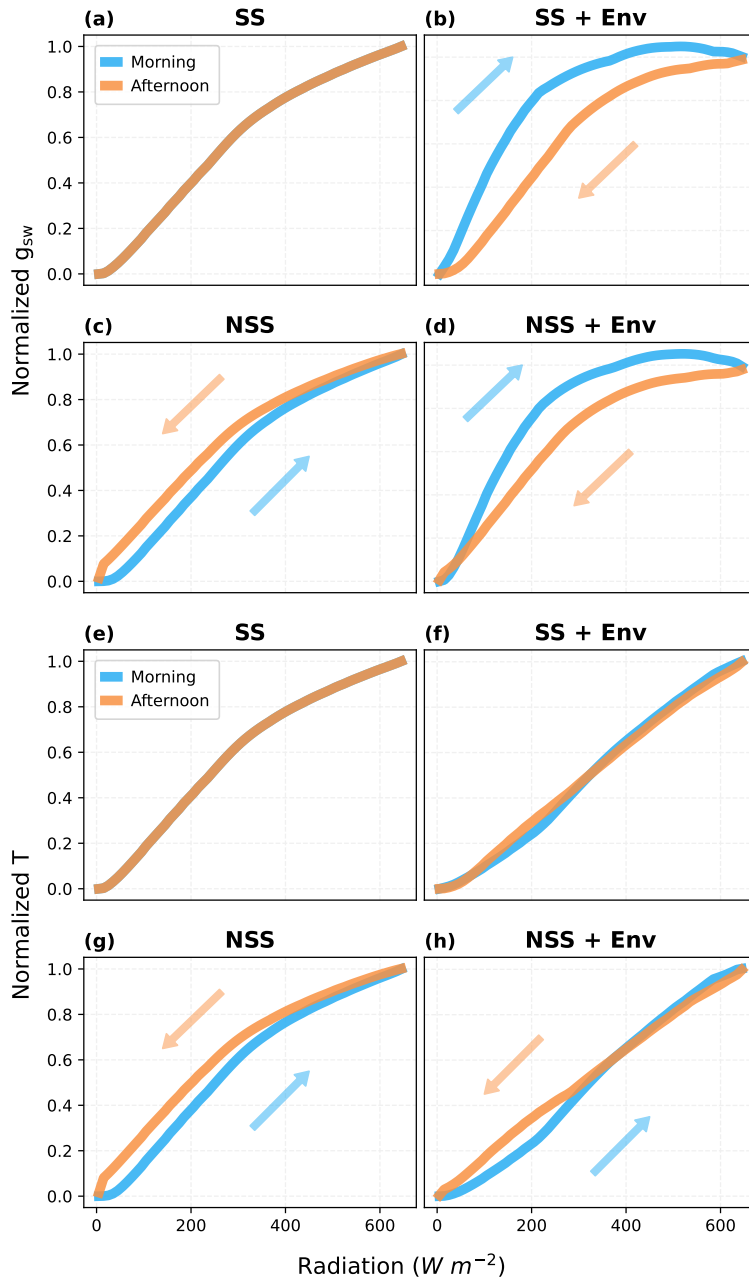
Figure S6: Hysteresis of the canopy-mean stomatal conductance (g_{sw}) and canopy transpiration rate (T) in response to radiation during an ideal clear-sky day, when $\tau_{op} = 300\,\text{s}$, $\tau_{cl} = 900\,\text{s}$. (a, e) SS model, (b, f) SS model with coupled diurnal variations of environmental conditions (Env, e.g. air temperature, VPD), (c, g) NSS model, (d, h) NSS model with Env. (a-d) normalized g_{sw} responses, (e-h) normalized T responses. In simulations without Env variations, except for the radiation, all the other environmental drivers were kept at the daytime means. g_{sw} and T is normalized with the values at noon (12:00). Arrows indicate the increasing and decreasing parts of the diurnal courses.
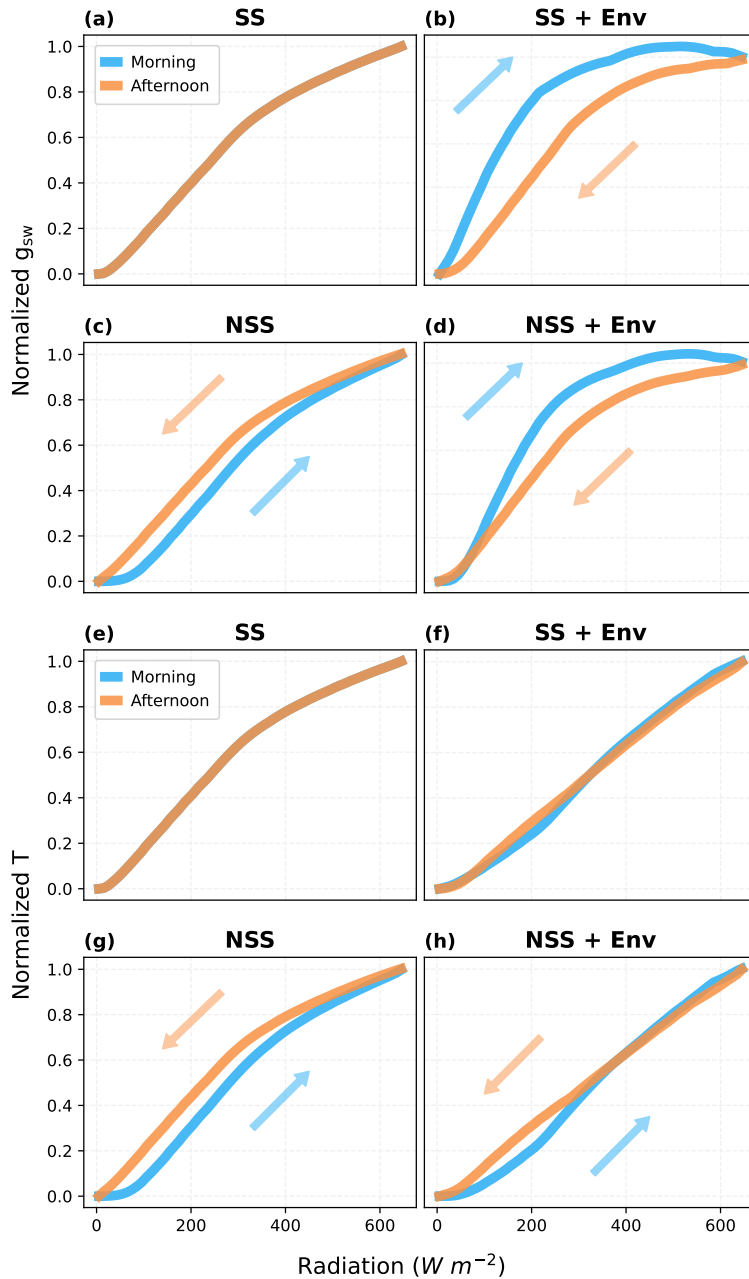
Figure S7: Hysteresis of the canopy-mean stomatal conductance (g_{sw}) and canopy transpiration rate (T) in response to radiation during an ideal clear-sky day, when $\tau_{op} = 900\,\mathrm{s}$, $\tau_{cl} = 300\,\mathrm{s}$. (a, e) SS model, (b, f) SS model with coupled diurnal variations of environmental conditions (Env, e.g. air temperature, VPD), (c, g) NSS model, (d, h) NSS model with Env. (a-d) normalized g_{sw} responses, (e-h) normalized T responses. In simulations without Env variations, except for the radiation, all the other environmental drivers were kept at the daytime means. g_{sw} and T is normalized with the values at noon (12:00). Arrows indicate the increasing and decreasing parts of the diurnal courses.

References

Butler, E. E., Datta, A., Flores-Moreno, H., Chen, M., Wythers, K. R., Fazayeli, F., Banerjee, A., Atkin, O. K., Kattge, J., Amiaud, B., Blonder, B., Boenisch, G., Bond-Lamberty, B., Brown, K. A., Byun, C., Campetella, G., Cerabolini, B. E. L., Cornelissen, J. H. C., Craine, J. M., Craven, D., de Vries, F. T., Díaz, S., Domingues, T. F., Forey, E., González-Melo, A., Gross, N., Han, W., Hattingh, W. N., Hickler, T., Jansen, S., Kramer, K., Kraft, N. J. B., Kurokawa, H., Laughlin, D. C., Meir, P., Minden, V., Niinemets, Ü., Onoda, Y., Peñuelas, J., Read, Q., Sack, L., Schamp, B., Soudzilovskaia, N. A., Spasojevic, M. J., Sosinski, E., Thornton, P. E., Valladares, F., van Bodegom, P. M., Williams, M., Wirth, C., and Reich, P. B.: Mapping local and global variability in plant trait distributions, Proceedings of the National Academy of Sciences, 114, E10 937–E10 946, https://doi.org/10.1073/pnas.1708984114, publisher: Proceedings of the National Academy of Sciences, 2017.

Croft, H., Chen, J. M., Wang, R., Mo, G., Luo, S., Luo, X., He, L., Gonsamo, A., Arabian, J., and Zhang, Y.: The global distribution of leaf chlorophyll content, Remote Sensing of Environment, 236, 111 479, iSBN: 0034-4257 Publisher: Elsevier, 2020.

De Kauwe, M. G., Kala, J., Lin, Y.-S., Pitman, A. J., Medlyn, B. E., Duursma, R. A., Abramowitz, G., Wang, Y.-P., and Miralles, D. G.: A test of an optimal stomatal conductance scheme within the CABLE land surface model, Geoscientific Model Development, 8, 431–452, https://doi.org/10.5194/gmd-8-431-2015, publisher: Copernicus GmbH, 2015.

Farquhar, G. D., von Caemmerer, S., and Berry, J. A.: A biochemical model of photosynthetic CO2 assimilation in leaves of C 3 species, Planta, 149, 78–90, https://doi.org/10.1007/BF00386231, number: 1, 1980.

He, L., Chen, J. M., Pisek, J., Schaaf, C. B., and Strahler, A. H.: Global clumping index map derived from the MODIS BRDF product, Remote Sensing of Environment, 119, 118–130, https://doi.org/10.1016/j.rse.2011.12.008, 2012.

Hersbach, H., Bell, B., Berrisford, P., Biavati, G., Horányi, A., Muñoz Sabater, J., Nicolas, J., Peubey, C., Radu, R., Rozum, I., et al.: ERA5 hourly data on single levels from 1979 to present, Copernicus climate change service (c3s) climate data store (cds), 10, 2018.

Luo, X., Keenan, T. F., Chen, J. M., Croft, H., Colin Prentice, I., Smith, N. G., Walker, A. P., Wang, H., Wang, R., Xu, C., and Zhang, Y.: Global variation in the fraction of leaf nitrogen allocated to photosynthesis, Nature Communications, 12, 4866, https://doi.org/10.1038/s41467-021-25163-9, number: 1 Publisher: Nature Publishing Group, 2021.

van der Tol, C., Verhoef, W., Timmermans, J., Verhoef, A., and Su, Z.: An integrated model of soil-canopy spectral radiances, photosynthesis, fluorescence, temperature and energy balance, Biogeosciences, 6, 3109–3129, https://doi.org/10.5194/bg-6-3109-2009, publisher: Copernicus GmbH, 2009.

Wang, Y., Braghiere, R. K., Longo, M., Norton, A. J., Köhler, P., Doughty, R., Yin, Y., Bloom, A. A., and Frankenberg, C.: Modeling Global Vegetation Gross Primary Productivity, Transpiration and Hyperspectral Canopy Radiative Transfer Simultaneously Using a Next Generation Land Surface Model—CliMA Land, Journal of Advances in Modeling Earth Systems, 15, e2021MS002 964, https://doi.org/10.1029/2021MS002964, _eprint: https://onlinelibrary.wiley.com/doi/pdf/10.1029/2021MS002964, 2023.

Yang, P., Verhoef, W., and van der Tol, C.: The mSCOPE model: A simple adaptation to the SCOPE model to describe reflectance, fluorescence and photosynthesis of vertically heterogeneous canopies, Remote Sensing of Environment, 201, 1–11, https://doi.org/10.1016/j.rse.2017.08.029, 2017.

Yuan, H., Dai, Y., Xiao, Z., Ji, D., and Shangguan, W.: Reprocessing the MODIS Leaf Area Index products for land surface and climate modelling, Remote Sensing of Environment, 115, 1171–1187, https://doi.org/10.1016/j.rse.2011.01.001, 2011.